Sonic Hedgehog Signaling (Shh) regulates the developmental shift of GABA polarity in rat somatosensory cortex

Abbreviated title: Smoothened receptor controls the GABA responses polarity

Authors Names and affiliations:

Quentin Delmotte[1,2,3], Igor Medina[1,2,3], Mira Hamze[1,2,3], Emmanuelle Buhler[2,5], Jinwei Zhang[6], Yesser H. Belgacem[2,3,#] and Christophe Porcher [1,2,3,#,*]

Co-last authors

[1]Aix-Marseille Univ, INSERM, INMED, Parc Scientifique de Luminy 13273, Marseille, France. [2]INSERM (Institut National de la Santé et de la Recherche Médicale) Unité 1249, Marseille, Parc Scientifique de Luminy, 13273 Marseille, France. [3]INMED (Institut de Neurobiologie de la Méditerranée), Parc Scientifique de Luminy, 13273 Marseille, France. [5]Plateforme Post-Génomique, INMED, 13273 Marseille, France. [6]University of Exeter Medical School, United Kingdom.

Authors Contributions: QD, IM, YHB and CP designed research. QD, IM, MH, EB, JW, YHB and CP performed research. QD, YHB and CP analyzed data. QD and CP wrote the paper.

[*]**Correspondence should be addressed to:**

Christophe Porcher, Ph.D., INMED, INSERM U1249, Parc scientifique de Luminy, BP 13, 13273 Marseille Cedex 09, France; Phone: 33 4 91 82 81 29; E-mail: Christophe.porcher@inserm.fr

Number of: Figures (7), Table (1), Multimedia (0)

Number of words: Abstract (184), Introduction (700), Discussion (1505).

Acknowledgements: We thank Drs. Y Ben Ari and J.L. Gaiarsa for critical reading of the manuscript; F. Michel at InMAGIC (INMED Imaging Centre) for technical assistance.

Conflict of interest: The authors declare no conflict of interest.

Funding: This work was supported by The National Institute of Health and Medical Research (INSERM), the National Center for Scientific Research (CNRS), the National Agency for Research (ANR, grant number R07066AS 2008-2011 to QD, CP and JLG and the A*MIDEX project (n° ANR-11-IDEX-0001-02) funded by the « Investissements d'Avenir » French Government program, managed by the French National Research Agency (ANR). IMERA/INSERM Grant, Marie Curie Prestige/ERC Grant (PRESTIGE-2016-3-0025) and Brain & Behavior Research Foundation (NARSAD) Young investigator grant (#25356) to YB.

ABSTRACT

Sonic Hedgehog (Shh) and its patched-smoothened receptor complex control a variety of functions in the early developing central nervous system (CNS) such as neural cell proliferation and differentiation. Recently, Shh signaling components have been found to be expressed at the synaptic level in the postnatal and adult brain, suggesting a potential role in the regulation of synaptic transmission. Here, using *in utero* electroporation of constitutively active and dominant-negative forms of the Shh co-receptor smoothened (Smo), we studied the role of Shh signaling in the development and maturation of GABAergic transmission in rat somatosensory cortex. Our results show that enhancing Smo activity during development accelerates, the shift from depolarizing to hyperpolarizing GABA, in a KCC2-dependent manner, rendering GABA inhibitory in immature tissues. On the other hand, blocking Smo activity maintains GABA response in a depolarizing state in mature cortical neurons resulting in altered chloride homeostasis and increased seizure susceptibility. Altogether, our study reveals an unexpected function of Shh signaling on the regulation of chloride homeostasis through the control of KCC2 trafficking and, in particular, on the timing of the GABA inhibitory/excitatory shift in brain maturation.

53 **Introduction**

54 Sonic hedgehog (Shh) is an activity-dependent secreted synaptic molecule (Beug et al., 2011). In the
55 presence of Shh ligand, receptor Patched-1 (PTCH1) relieves its constitutive inhibition on G-protein
56 coupled co-receptor Smoothened (Smo), leading to activation of downstream signaling factors (Riobo
57 et al., 2006; Briscoe and Thérond, 2013; Belgacem and Borodinsky, 2015). The Shh signaling
58 pathway plays a wide range of functions during embryonic development from neuronal cell
59 proliferation to differentiation (Traiffort et al., 2010; Ruat et al., 2012; Briscoe and Thérond, 2013;
60 Belgacem et al., 2016). Furthermore, in the developing mammalian central nervous system, Shh
61 signaling is involved in axonal elongation (Hammond et al., 2009; Parra and Zou, 2010; Yao et al.,
62 2015) and formation of the cortical connectivity (Harwell et al., 2012; Memi et al., 2018). After birth,
63 Shh signaling components have been found in several brain regions, including the cerebral cortex and
64 hippocampus, from an early stage of postnatal development to adulthood (Charytoniuk et al., 2002;
65 Traiffort et al., 2010; Petralia et al., 2011, 2012; Rivell et al., 2019). In the adult hippocampus, Shh
66 plays an essential role in neurogenesis in the dentate gyrus (Breunig et al., 2008; Antonelli et al.,
67 2019). In addition, Shh receptors PTCH1 and Smo are also expressed at the synaptic junction of the
68 immature and adult hippocampus (Charytoniuk et al., 2002; Petralia et al., 2011; Mitchell et al., 2012),
69 suggesting other roles than control of neurogenesis (Zuñiga and Stoeckli, 2017). For instance, Shh was
70 reported to exert a modulatory action on neuronal electrical activity in the adult brain (Bezard et al.,
71 2003; Pascual et al., 2005) and more recently Shh signaling has been shown to regulates the formation
72 of glutamatergic and GABAergic terminals in hippocampal neurons (Mitchell et al., 2012). These
73 morphological changes were accompanied by an increase in the frequency of excitatory postsynaptic
74 currents (Mitchell et al., 2012; Feng et al., 2016). Altogether, these findings support the view that Shh
75 signaling pathway plays a crucial role during early postnatal neuronal circuit construction and synaptic
76 plasticity in the hippocampus and cortex. Thus, its impairment may affect neuronal network formation
77 and lead to brain dysfunction. Likewise, both in human and animal models accumulating evidences
78 indicate that impairment of Shh pathway at postnatal stages may contribute for the emergence of
79 neurodevelopmental disorders, including autism spectrum disorders (Al-Ayadhi, 2012; Halepoto et al.,
80 2015) and seizures (Feng et al., 2016; Su et al., 2017).

81 In the early postnatal life, the $GABA_A$ receptor function changes from depolarizing to
82 hyperpolarizing in a KCC2 dependent manner (Ben-Ari et al., 1989; Rivera et al., 1999). Alteration in
83 the GABA developmental sequence leads to compromised balance between excitatory and inhibitory
84 transmission associated with severe changes in the neuronal network circuitry (Ben-Ari, 2002; Ben-
85 Ari et al., 2007; Wang and Kriegstein, 2009; Sernagor, 2010; Kilb et al., 2013) and subsequently,
86 onset of neurodevelopmental brain disorders such as ASD, epilepsy or schizophrenia (Ben-Ari and
87 Holmes, 2005; Kuzirian and Paradis, 2011; Mueller et al., 2015).
88 Although both Shh and earlier GABA signaling are critically involved in similar processes of
89 neuronal network formation and are implicated in etiology of same neurodevelopmental disorders,
90 their putative interplay remains unclear. Here we postulated that Shh components may contribute to
91 the onset of the GABA polarity shift and suggested that deregulation of Shh signalling pathway may
92 then lead to an impaired neuronal network and to the emergence of brain disorders at adulthood.
93 Because loss of function of Smo have an embryonic lethal phenotype (Zhang et al., 2001) and Smo
94 activation in Wnt1-Cre;R26SmoM2 mice induces a hyperplasia of the facial processes at embryonic
95 stages (Jeong et al., 2004), we used in utero electroporation (IUE) to target the somatosensory cortex
96 with constructs encoding either for the dominant-negative (Smo Δ570-581) (Kim et al., 2009) or the
97 constitutively active (Smo A1) (Chen et al., 2011) Smo variants. Our results reveal an unexpected
98 function for Shh/PTCH/Smo signaling pathway in the regulation of GABAergic developmental timing
99 in the rat cerebral cortex, notably through the modulation of KCC2 cell surface expression and
100 stability. We further show that impairment of Shh signaling maintains a depolarizing action of GABA,
101 which then leads to an alteration of GABAergic inhibitory transmission in adulthood and may
102 contributes to the emergence of brain disorders.
103

Material and methods

All animal procedures were carried out according to the guidelines set by the INSERM animal welfare through the local committee (CEEA n°14) and the European Communities Council Directives (2010/63/UE). Male and female Wistar rats were purchased from Janvier Labs (https://www.janvier-labs.com/fiche_produit/rat_wistar/). Animals were raised and mated at INMED A2 animal facility housed under a 12 h light/dark cycle at 22-24°C and had access to food and water *ad libitum*.

Reagents and treatments

The following reagents were purchased from the indicated sources: 1,2,3,4-Tetrahydro-6-nitro-2,3-dioxo-benzo[f]quinoxaline-7-sulfonamide (NBQX) was obtained from the Molecular, Cellular and Genomic Neuroscience Research Branch (MCGNRB) of the National Institute of Mental Health (NIMH, Bethesda, MD, USA). TTX was purchased from abcam (Cambridge, UK). Isoguvacine, bicuculline and VU0463271 were purchased from Tocris Cookson (Bristol, UK). Strychnine and Bumetanide from Sigma (St-Louis, Missouri, USA).

In utero electroporation

In utero injections and electroporations were performed in embryos from timed pregnant rats (embryonic day 15) that received buprenorphine (Buprecare at 0.03 mg/kg) and were anaesthetized with sevoflurane (4.5%) 30 minutes later (Martineau et al., 2018). Briefly, the uterine horns were exposed, and a lateral ventricle of each embryo was injected using pulled glass capillaries and a microinjector (PV 820 Pneumatic PicoPump; World Precision Instruments, Sarasota, FL) with Fast Green (2 mg/ml; Sigma, St Louis, MO, USA) combined with the following DNA constructs encoding GFP or mCherry and/or Smo Δ570-581 (Kim et al., 2009) and/or Smo A1 (Chen et al., 2011) and/or Cl-Sensor (ratio 1:2). Plasmids were further electroporated by delivering 40V voltage pulses with a BTX ECM 830 electroporator (BTX Harvard Apparatus, Holliston, MA, USA). The voltage was discharged in five electrical pulses at 950 ms intervals via tweezer-type electrodes (Nepa Gene Co, Chiba, Japan) placed on the head of the embryo across the uterine wall. We

131 performed *in utero* electroporation in embryonic rats at E15, corresponding to an active period of both
132 radial and tangential migration of newborn neurons in the cortex (Kriegstein and Noctor, 2004). At
133 birth, successfully electroporated pups were selected after transcranial visualization of the
134 GFP reporter fluorescent proteins only. Following experimentation, morphological analysis of
135 electroporated tissues, selected by GFP or mCherry expression under fluorescent stereomicroscope
136 (Olympus SZX 16), was performed. The criteria commonly used for exclude animals were:
137 localization and cell density of transfected cortices and absence of abnormal cortex morphology (i.e.
138 cortical disruption, thickening and abnormal cortical organization). Our analyses revealed no
139 alterations in cortical layer position or morphology in GFP, mCherry, SmoA1 and Smo Δ570-581
140 conditions, although we cannot exclude the possibility that Smo constructs impact the neuronal cells at
141 the cellular and subcellular levels. Nevertheless, approximately 20% of electroporation failed due to
142 the absence of transfected cells as revealed by the lack of fluorescent cells (in GFP or mCherry and
143 Smo conditions). These animals were excluded from the study.
144
145 ***Western blotting***
146 Electroporated zones of the somatosensory cortex were homogenized in RIPA buffer (150 mM NaCl,
147 1% Triton X100, 0,1% SDS, 50 mM Tris HCl, pH 8, containing protease inhibitors (Complete Mini;
148 Roche). Lysates were centrifuged (10.000g for 10 min at 4°C) and the supernatant was heated at 90°C
149 for 5 min with Laemmli loading buffer. Loading was 20 µg of proteins as determined using a modified
150 Bradford reaction (BioRad Laboratories). Proteins were separated in 7–15% SDS-PAGE and
151 electrophoretically transferred to nitrocellulose membranes. Membranes were blocked with 5%
152 Bovine Serum Albumin (BSA) in TBS 0,1% Tween 20 (TBST) for 2h at RT, then incubated with
153 primary antibodies diluted in TBST containing 3% BSA overnight at 4°C or 2h at RT. Blots were
154 probed with antibody against KCC2 (1:2000; rabbit, US Biological), NKCC1 total (1mg/ml; Sheep,
155 S022D, Division of Signal Transduction Therapy Unit (DSTT), University of Dundee UK) and tubulin
156 (1:10.000; ß-tubulin, mouse, Sigma). After washing with TBST, membranes were incubated with
157 HRP-conjugated secondary antibodies diluted in TBST containing 3% BSA for 60 min, washed with

158 TBST and then developed using the G:BOX gel imaging system (Syngene). The appropriate exposure
159 time of the digital camera for acquisition of chemiluminescent signals from immunoblots was adapted
160 to avoid saturated pixels and expression levels were estimated by Image J software (NIH, Bethesda,
161 MD; http://rsb.info.nih.gov/ij/).
162
163 ***Immunocytochemistry and confocal microscopy***
164 Under deep anesthesia with isoflurane prior to chloral hydrate (7% in PBS 1M), P10 to P30
165 electroporated rats were intracardially perfused with cold PBS (1M) followed by 4% PFA in PBS.
166 Brains were removed, post-fixed overnight at 4°C and rinsed in PBS. Coronal cortical sections (70µm
167 thick) were obtained using a vibratome (Microm HM 650V). Sections were incubated first for 1 h in
168 PBS with 1% BSA and 0.3% Triton X-100, then overnight at 4°C with rabbit anti-Smo (1:500;
169 ab38686; Abcam) or rabbit anti-caspase-3 cleaved (1:500; 9661S; Cell Signaling) or chicken anti-
170 MAP2 (1:5000; ab5392; Abcam) or mouse anti-NeuN (1:1000; MAB377; Chemicon), or rabbit anti-
171 FoxP2 (1:4000; ab16046; Abcam), or mouse anti-synaptophysin (1:000; MAB5258; Chemicon).
172 Sections were rinsed in PBS and incubated for 2h with the corresponding Alexa488 (1:1000;
173 FluoProbes), Cy5 or Cy3-conjugated secondary antibodies diluted in PBS (1:1000; Chemicon). DAPI
174 staining was applied for nuclear localization (Vector Laboratories H-1200). Control tissues used to
175 determine the level of nonspecific staining included tissues incubated without primary antibody.
176 Sequential acquisition of immunoreactivity of GFP positive pyramidal-like cells was performed using
177 laser scanning confocal microscope (Zeiss LSM 510 Meta) with a 40X or 63X oil-immersion
178 objectives. For each experimental condition, a semi-quantitative analysis of Synaptophysin (Syn)
179 labeled area fraction per field was measured and reported to the area fraction of positive pixels for
180 MAP2. The surface areas of NeuN immuno-positive neurons expressing GFP or Smo-related
181 constructs were measured manually using the Freehands selection tool in Image J. In each set of
182 images, laser light levels and detector gain and offset were adjusted to avoid any saturated levels.
183 Optical sections were digitized (1024 × 1024 pixels) and processed using Image J software. All of the
184 images were analyzed blindly.
185

186 ***Relative Quantitative Expression of mRNA transcripts***

187 Expressions of Gli1 and PTCH1 mRNA in the electroporated regions of the somatosensory cortex
188 were measured by real-time quantitative RT-PCR. Total RNAs were isolated from cerebral cortices
189 (P15 rats) using Mini RNeasy kit (Qiagen) then converted to cDNA using 1 µg RNA and a QuantiTect
190 Reverse Transcription kit (Qiagen) according to manufacturer's instructions. PCR was carried out with
191 the LightCycler 480 SYBR Green I Master (Roche Applied Science) with 1 µL cDNA using the
192 following oligonucleotides (QuantiTect Primer Assays, Qiagen): Gli1 (Gli1; QT01290324), PTCH1
193 (QT01579669), and glyceraldehyde-3-phosphate dehydrogenase (GAPDH; QT001199633).
194 Quantitative RT-PCR was performed with a Roche LC480 Light Cycler (Roche Applied Science)
195 following the manufacturer's instructions. Relative mRNA values were calculated using the LC480
196 software and GAPDH as the housekeeping gene. PCR was performed in replicates of 3.

197

198 ***Slices preparation and electrophysiological recordings***

199 Somatosensory electroporated cortical slices identified by the atlas of Paxinos and Watson (Paxinos
200 and Watson, 2005) were prepared from P30 rats in ice-cold (2-4°C) oxygenated modified artificial
201 cerebrospinal fluid (ACSF) (0.5mM CaCl2 and 7mM MgSO4; NaCl replaced by an equimolar
202 concentration of choline). Slices (300 µm thick) were cut with a Vibratome (VT1000E; Leica,
203 Nussloch, Germany) and kept at room temperature (25°C) for at least one hour before recording in
204 oxygenated normal ACSF containing (in mM): 126 NaCl, 3.5 KCl, 2 $CaCl_2$, 1.3 $MgCl_2$, 1.2 NaH_2PO_4,
205 25 $NaHCO_3$ and 11 glucose, pH 7.4 equilibrated with 95% O_2 and 5% CO_2. Slices were then
206 transferred to a submerged recording chamber perfused with ACSF (3 mL/min) at 34°C.

207

208 ***Spiking activity and data analysis***

209 Extracellular field potential recordings were performed from P14, P20 and P30 electroporated
210 somatosensory cortical slices. Extracellular tungsten electrodes of 50µm diameter (California Fine
211 Wire, Grover Beach, CA, USA) were positioned in the V/VI cortical pyramidal cell layer of the
212 transfected area to record the Multi Unit Activity (MUA). Field potentials were recorded using a
213 DAM80 Amplifier (World Precision Instruments, Sarasota, FL, USA) using a 1–3 Hz bandpass filter

214 and analyzed off-line with the Axon package MiniAnalysis program (Jaejin Software, Leonia, NJ,
215 USA). To determine the developmental changes in the $GABA_A$ signaling, we used isoguvacine, a
216 potent and selective $GABA_A$ receptor agonist (Krogsgaard-Larsen and Johnston, 1978). We
217 determined the effect of isoguvacine on MUA as a ratio of the spiking frequency at the peak of the
218 isoguvacine response to the spiking frequency in control.
219
220 ***Cl⁻-Sensor fluorescence recordings from brain slices***
221 To perform a non-invasive monitoring of $[Cl^-]_i$ we used a ratiometric genetically-encoded Cl^--sensitive
222 probe called Cl-Sensor (Markova et al., 2008; Waseem et al., 2010) that was co-expressed into the
223 cells of interest together with other constructs as described above. The acquisition of fluorescence
224 images was performed using a customized imaging set-up and consecutive cells excitation at 430 and
225 500 nm and emission at 480 and 540 nm. The frequency of acquisition was 0.05 Hz. The duration of
226 excitation was selected for each cell type and was selected to avoid use-dependent bleaching of the
227 signal (Friedel et al., 2013). Results are expressed as ratio R430/500. Experiments were performed on
228 acute cortical slices from *in utero* electroporated rat pups on postnatal days P10 and P30.
229 Electroporated cortical regions of the P10 rat were identified using an atlas of the developing rat brain
230 (Khazipov et al., 2015). Electroporated cortical regions of the P30 rat were identified using the
231 Paxinos and Watson rat brain atlas (Paxinos and Watson, 2005). Based on these two atlases, the
232 somatosensory regions were used for acute slice experiments. Individual slices were transferred to a
233 specially designed recording chamber where they were fully submerged and superfused with
234 oxygenated ACSF complemented with 1 μM tetrodotoxin, 0.3 μM strychnine, and 10 μM NBQX to
235 prevent spontaneous neuronal activity and noncontrolled $[Cl^-]_i$ changes at 30–32°C at a rate of 2–3
236 ml/min. The applications of the ACSF solution containing isoguvacine (30 μM) or KCl (25 mM) +
237 isoguvacine (30 μM) were performed with a perfusion system.
238
239 ***Seizure induction with pentylenetetrazol (PTZ)***
240 To evaluate the susceptibility to seizures in controls rats (GFP-transfected brains), in SmoA1 and Smo
241 Δ570-581 animals at P30, PTZ (25 mg/kg; Sigma) was administered via intraperitoneal injections

242 every 10 min until generalized seizures occurred. Rats were placed in a plexiglass cage and the time to
243 the onset of the generalized seizure was measured by observation. There was no significant difference
244 in weight and sex between groups of animals. Experiments were done blind and electroporated region
245 was verified after PTZ induction. Rats with a very focal fluorescence or fluorescence in other brain
246 regions than somatosensory cortex were excluded.
247
248 ***Primary cultures and transfection of rat hippocampal neurons***
249 Neurons from 18-day-old rat embryos were dissected and dissociated using trypsin and plated at a
250 density of 70,000 cells cm^{-2} in minimal essential medium (MEM) supplemented with 10% NU serum
251 (BD Biosciences, Le Pont de Claix, France), 0.45% glucose, 1 mM sodium pyruvate, 2 mM glutamine
252 and 10 U ml−1 penicillin–streptomycin (Buerli et al., 2007). On days 7, 10 and 13 of culture
253 incubation (DIV, days *in vitro*), half of the medium was changed to MEM with 2% B27 supplement
254 (Invitrogen). For electrophysiology neuronal cultures were plated on coverslips placed in 35-mm
255 culture dishes. Twelve hours before plating, dishes with coverslips were coated with polyethylenimine
256 (5 mg/ml). Transfection of cultured neurons was performed with 300 µl Opti-MEM medium mixed
257 with 7 µl Lipofectamine 2000 (Invitrogen), 1 µl Magnetofection CombiMag (OZ Biosciences) per µg
258 of DNA and 1.5 µg premixed DNAs encoding constructs of interest. The mixture was incubated for 20
259 min at room temperature and thereafter distributed dropwise above the neuronal culture. Culture
260 dishes (35-mm) were placed on a magnetic plate (OZ Biosciences) and incubated for 35 min at 37°C,
261 5% CO_2. Transfection was terminated by the substitution of 80% of the incubation solution with fresh
262 culture medium. Cells were used in the experiments 48-72 hours after transfection. These experiments
263 were based on co-transfection into the same cell of two different pcDNAs encoding a fluorescent
264 marker of transfection (eGFP or mCherry, 0.3 µg), and Smo related-constructs (1.2 µg).
265
266 **Gramicidin-perforated patch-clamp recordings**
267 Gramicidin-perforated patch-clamp recordings were performed on primary hippocampal neurons,
268 transfected with a mixture of constructs encoding mCherry (mock) or Smo Δ570-581 or Smo A1 with
269 or without KCC2-pH_{ext} (Friedel et al., 2017). Measurements were performed 2 or 3 days after

270 transfection (corresponding to 8 or 9 DIV). Coverslips with transfected neurons were placed onto the
271 inverted microscope and perfused with an external Hepes-buffered solution (HBS) (in mM): 140
272 NaCl, 2.5 KCl, 20 Hepes, 20 d-glucose, 2.0 $CaCl_2$, 2.0 $MgCl_2$, and 0.02 Bumetanide, pH 7.4. For
273 recording from neurons, external HBS contained 0.5 µM tetrodotoxin and 15 µM bumetanide. The
274 recording micropipettes (5 MΩ) were filled with a solution containing (in mM): 150 KCl, 10 Hepes,
275 and 20 µg/ml gramicidin A, pH 7.2. Isoguvacine (30 µM) was dissolved in external solution and
276 focally applied to recorded cells through a micropipette connected to a Picospritzer (General Valve
277 Corporation, pressure 5 p.s.i.). Recordings were done using an Axopatch-200A amplifier and
278 pCLAMP acquisition software (Molecular Devices) in voltage-clamp mode. Data were low-pass
279 filtered at 2 kHz and acquired at 10 kHz. Isoguvacine responses were recorded at voltages -110, -90, -
280 70 and -50 mV or at -70, -50, -30 and -10 mV depending on neuron GABA inversion potential. A
281 linear regression was used to calculate the best-fit line of the voltage dependence of the isoguvacine
282 responses.
283
284 ***Surface immunolabelling on living neurons and analysis of KCC2-pH$_{ext}$ proteins***
285 For immunolabelling of KCC2-pH$_{ext}$ proteins on living neurons, rabbit anti-GFP antibody were
286 dissolved in culture media applied to neurons for 2 hours at 37°C, 5% CO2 (Friedel et al., 2015).
287 Neurons were then rinsed three times at room temperature (RT) with HBS, labeled with anti-rabbit
288 Cy3-conjugated antibody for 20 min at 13°C and fixed in Antigenfix (Diapath). To reveal intracellular
289 pool of live-labelled proteins, cells were permeabilized with 0.3% Triton X-100, blocked by 5% goat
290 serum and incubated during 1 h at RT with anti-rabbit Alexa 647-conjugated antibody. For
291 visualization of the total pool of overexpressed KCC2-pH$_{ext}$ cells were labeled overnight (4°C) with
292 mouse anti-GFP antibody and for 1 hour at RT with anti-chicken Alexa 488-conjugated antibody. For
293 control of the cell integrity during live-cell immunolabelling, one batch of cultures were routinely
294 transfected with KCC2-pH$_{ext}$ mutant ΔNTD-KCC2-pH$_{ext}$ that does not incorporate into the plasma
295 membrane (Friedel et al., 2017).
296 Images of labeled neurons were acquired with an Olympus Fluorview-500 confocal microscope
297 (oil-immersion objective 60x (NA1.4); zoom 1-5). We randomly selected and focused on a transfected

298 cell by only visualizing Alexa-488 fluorescence and then acquired Z-stack images of Alexa-488, CY3
299 and Alexa-647 fluorochromes. Each Z-stack included 10 planes of 1 µm optical thickness and taken at
300 0.5 µm distance between planes. The cluster properties and fluorescence intensities of each cell were
301 analyzed with Metamorph software. First, we used the logical "NOT" conversion of pairs of Alexa-
302 647 and CY3 images to isolate in each focal plane the Alexa-647 signal that was not overlapping with
303 CY3 fluorescence restricted to plasma membrane. This gave rise to additional images reflecting the
304 fluorescence of the internalized pool of labeled clusters, called thereafter "NOT-conversion". Second,
305 the arithmetic summation for each Z-stack and channel was performed to collect the whole
306 fluorescence of the different signals (Alexa-488 = total protein fluorescence; CY3 = plasma membrane
307 restricted fluorescence; NOT-conversion = internalized restricted fluorescence; Alexa-647 = all
308 surface labeled fluorescence). Third, a binary mask was created for each cell from Alexa-488 image to
309 isolate the signal coming from the transfected neuron, and the fluorescence parameters (total
310 fluorescence, single cluster fluorescence as well as density and brightness of clusters) were analyzed
311 for each channel (Alexa-488, CY3, NOT-conversion and Alexa-647) in regions overlapping with the
312 binary mask. The analysis parameters were the same for each experiment and all experiments were
313 done blind. After analysis, data were normalized to the mean value of cells transfected with KCC2-
314 pHext + GFP.
315
316 ***Statistical analysis***
317 No statistical methods were used to predetermine sample sizes. To ensure the consistency and
318 reproducibility of our results, we conducted repeated trials in different cell cultures and acute brain
319 slices prepared from at least three different animals for each experimental condition. If not stated
320 otherwise, statistics are presented as the mean ± the standard deviation (SD) for normaly distributed
321 data and as the median only for non-normaly distributed data. Experiments with control and Smo
322 electroporated animals were processed at the same time to ensure homogeneity of experimental
323 conditions. Statistical analyses and assessment of normal distribution (Shapiro-Wilk test) were
324 performed with GraphPad Prism (GraphPad software 5.01). For data showing normal distribution,
325 ANOVA and the post hoc Tukey test were used for multiple comparisons between groups, and a

paired t-test was used to compare paired data. For data displaying non-normal distribution Kruskal-Wallis test was used to compare three of more independent groups, Mann-Whitney U-test was used for comparison between 2 independent groups and Wilcoxon matched-pairs signed rank test to analyze differences within one group across conditions. Details of the statistical analysis are summarized in Table 1.

354 **Results**

355 ***Cortical expression pattern of Smo A1 and* Smo Δ570-581**

356 Previous studies have shown that Shh signaling pathways components, including PTCH and Smo, are
357 present in the postnatal mammalian brain (Petralia et al., 2011; Harwell et al., 2012; Mitchell et al.,
358 2012; Rivell et al., 2019). In the mouse neocortex, Shh signaling pathway regulates the formation of
359 neuronal network in immature brain, suggesting that Shh signaling components may play a major role
360 in construction and maturation of neural circuits during the postnatal periods. In order to evaluate the
361 potential role of Shh in the developing brain, we used IUE of plasmids to express GFP or mCherry
362 alone as controls or in combination with constitutively active (Smo A1) or dominant-negative (Smo
363 Δ570-581) forms of Smo, an essential component for Shh signaling. IUE of rat brains was performed
364 at embryonic day 15 (E15) in order to target mainly pyramidal neurons of the layers V/VI (Kriegstein
365 and Noctor, 2004). Coronal sections through the somatosensory cortex of GFP or mCherry and Smo-
366 related constructs co-electroporated tissues from P15 rodents were immunolabeled with neuronal
367 markers NeuN and FoxP2 (deeper layer neurons markers) to assist in the histological identification of
368 cortical layers (Fig. 1A). The fluorescence intensity profile of both Smo A1 and Smo Δ570-581
369 expressing neurons does not show any obvious differences in the cortical layering when compared to
370 control GFP or mCherry-expressing cells. Thus, Smo A1 or Smo Δ570-581 expressing neurons
371 electroporated at E15 most likely represent the layers V/VI of the somatosensory cortex.

372 Because Shh signaling is involved in cell division and cell growth of cerebral cortex
373 progenitors (Araújo et al., 2014), we investigated whether Smo-related constructs could impact the
374 cortical thickness or the neuronal cell density and size in electroporated tissues. We found that cortical
375 thickness of Smo A1 and Smo Δ570-581 rats does not present any difference compared to control rats
376 (median values: 1772 µm, 1779 µm and 1772 µm respectively; p=0.07 between Smo A1 and CTRL
377 rats, p=0.17 between Smo Δ570-581 and CTRL, Mann-Whitney test; Fig. 1B). The density of NeuN
378 immuno-positive cells in Smo A1 and Smo Δ570-581 electroporated somatosensory cortices,
379 measured in the layer V, reveals no difference when compared to control tissues (46 neurons per
380 observation field for CTRL, vs 41 for Smo A1; p = 0.72 and 41 neurons for Smo Δ570-581; p = 0.44,
381 Mann-Whitney test; Fig. 1C). Similarly, the average soma neuronal size remains unchanged (210,3

382 µm² for CTRL vs 229.2 µm ² for Smo A1 and 213.8 µm² for Smo Δ570-581; p=0.26 and p=0.48
383 between CTRL and Smo Δ570-581, Mann-Whitney test; Fig. 1D).

384 In hippocampal neurons, exogenous treatment with Shh or Smo agonist (SAG) upregulate
385 presynaptic nerve terminals (Mitchell et al., 2012). Theses observations led us to investigate whether
386 Smo A1 or Smo Δ570-581 could modulate the density of presynaptic terminals in electroporated
387 cortices. In order to assess the possible changes at the presynaptic levels, we performed quantitative
388 analysis of the area fraction of synaptophysin on MAP2-positive neurons at P30. Compared with
389 control GFP, Smo Δ570-581 electroporated tissues showed a significant decrease in the area fraction
390 of synaptophysin immunolabeling (16.05 % for Smo Δ570-581 vs 19.67 % for CTRL; p = 0.01,
391 Mann-Whitney test; Fig. 1E), whereas Smo A1 increased the area fraction of synaptophysin-positive
392 synapses (24.77 % for Smo A1; p = 0.01 when compared to CTRL and $p < 0.0001$ when compared to
393 Smo Δ570-581, Mann-Whitney test; Fig. 1E).

394 Recent evidences indicate that Smo signaling pathway inhibits neuronal apotosis (Wang et al.
395 2018), whereas loss of Smo activity leads to increased neuronal apoptosis (Qin, Suping, 2019). In
396 order to assess if Smo A1 or Smo Δ570-581 induces apoptosis in electroporated neurons, we
397 performed immunohistochemical analysis for cleaved caspase-3, a marker for cell apoptosis (Logue
398 and Martin, 2008) on electroporated rats at P15. Quantification of cleaved caspase-3-positive neurons
399 shows no significant difference between the constitutively active mutant (0.24 ± 0.13 % and 0.34 ±
400 0.23 % in respectively Smo A1 and CTRL; p = 0.70, Mann-Whitney test; Fig. 1F and G), or dominant
401 negative (0.23 ± 0.15; p = 0.74, Mann-Whitney test; Fig. 1F and G) forms of Smo when compared to
402 GFP control tissues.

403 All together, these observations indicate that expression of constitutively active or dominant
404 negative forms of Smo does not alter the mean neuronal density and the positioning of pyramidal
405 neurons in the cerebral cortex. Moreover, these results also suggest that *in utero* electroporation of the
406 constitutively active or dominant-negative forms of Smo does not affect apoptosis mechanisms in the
407 postnatal cerebral cortex. By contrast, both Smo A1 and Smo Δ570-581 modify significantly the
408 formation of synaptic terminals. In keeping with previous findings showing Smo-dependent
409 enhancement of synapse formation (Mitchell et al., 2012) our results indicate that Smo A1 and Smo

410 Δ570-581 electroporation is an effective strategy to modify Shh signaling pathway.

411

412 **Smo-related constructs regulate the expression levels of its downstream target genes**

413 To investigate the functional expression of the two Smo-related constructs, we performed
414 immunofluorescence labeling by using antibody raised against Smo protein in somatosensory cortical
415 tissues overexpressing Smo A1 or Smo Δ570-581 constructs at P15. As illustrated in figure 2A, the
416 anti-Smo antibody detected well the expression of Smo A1 and Smo Δ570-581 in the electroporated
417 somatosensory cortex. Smo activation mobilizes activator forms of Gli transcription factors, which in
418 turn lead to an increase of PTCH1 and Gli1 expression (Jacob and Lum, 2007). In order to validate
419 functional expression of Smo A1 or Smo Δ570-581, we quantified Gli1 and PTCH1 mRNA levels in
420 cortices overexpressing Smo A1 or Smo Δ570-581 mutants using qRT-PCR at P15. As expected, Gli1
421 mRNA expression levels are increased in Smo A1 when compared with GFP control animals (CTRL)
422 (median values: 1.39 vs 0.76 a.u. in respectively Smo A1 and CTRL; $p = 0.041$, Mann-Whitney test;
423 Fig. 2B), and conversely decreased in Smo Δ570-581 (0.48 a.u.; $p = 0.039$ when compared to CTRL,
424 Mann-Whitney test; Fig. 2B). When compared with CTRL and Smo A1 animals, PTCH1 mRNA
425 transcripts are downregulated in Smo Δ570-581 rats (3.61 a.u. in Smo Δ570-581 vs 6.97 a.u. in CTRL
426 and 6.21 a.u. in Smo A1; $p = 0.026$ when compared Smo Δ570-581 to CTRL; $p = 0.008$ when
427 compared Smo Δ570-581 to Smo A1, Mann-Whitney test; Fig. 2C). No significant difference is
428 observed for PTCH1 mRNA levels between CTRL and Smo A1 (6.21 a.u. for Smo A1; $p = 0.66$,
429 Mann-Whitney test; Fig. 2C).

430 These results confirm that in the electroporated tissues, the constitutively active SmoA1
431 significantly promotes the expression of the target gene Gli1 whereas the dominant negative Smo
432 Δ570-581 acts in an opposite way by reducing its expression.

433

434 ***Smo-dependent Shh signaling controls the developmental GABA excitatory to inhibitory shift***

435 Cortical neuronal network construction during postnatal period requires the depolarizing to
436 hyperpolarizing shift of GABA to occur at a precise timing during maturation (Ben-Ari and Holmes,
437 2005; Wang and Kriegstein, 2009; Wu and Sun, 2015). Because Shh signaling plays a nodal role in

438 brain development (Álvarez-Buylla and Ihrie, 2014; Yao et al., 2016), we investigated whether the
439 manipulation of Smo activity will affect the onset of GABA excitatory/inhibitory postnatal shift at the
440 network level. We performed field recordings of MUA in acute cortical slices from control (GFP)-,
441 Smo A1- and Smo Δ570-581 rats and measured the effect of bath application of the $GABA_AR$ agonist
442 isoguvacine (10 μM) on their spiking activity at P14, P20 and P30. Accordingly to the known
443 depolarizing action of GABA in the immature neocortex (Kirmse et al., 2015; Riffault et al., 2018),
444 isoguvacine induced an increase of spiking activity at P14 in cortical slices from control and Smo
445 Δ570-581 dominant negative rodents (median values: +33.87 %; p = 0.019 and +86.12 %; p = 0.019
446 respectively, Wilcoxon matched-pairs signed test; Fig. 3A and B). In contrast, isoguvacine decreased
447 the spiking activity in Smo A1 constitutively active mutants (-12 %; p = 0.009, Wilcoxon matched-
448 pairs signed test, Fig. 3A and B). At P20, isoguvacine induced either a decrease or an increase of
449 spiking activity in control (-11.37 %; p = 0.519, Wilcoxon matched-pairs signed test; Fig. 3B). In
450 slices obtained from Smo A1 rats we observed a decrease of spikes frequency, while in Smo Δ570-581
451 condition, isoguvacine induced a strong increase of spikes frequency (-47.03 %; p = 0.011 and
452 +60.21%; p = 0.042 respectively, Wilcoxon matched-pairs signed test; Fig. 3B). At P30 (Fig. 3A, B
453 and C), isoguvacine induced a decrease in spikes frequency from control and Smo A1 cortical slices,
454 whereas it increases the spiking activity in Smo Δ570-581 rats (-22.86 %; p = 0.0078, -42.15 %; p =
455 0.015 and +12.89 %; p = 0.015 respectively, Wilcoxon matched-pairs signed test; Fig. 3A and B).
456 Thus, the overall effects of isoguvacine on the spiking activity in the electroporated cortical slices
457 suggest that Smo A1- and Smo Δ570-581-related construct accelerates and delays respectively the
458 developmental hyperpolarizing GABA shift ($p<0.0001$, Chi-square test; Fig. 3C).

459 To investigate if early GABAergic maturation in Smo A1 rats is KCC2 or NKCC1-dependent,
460 we applied the KCC2-selective blocker VU0463271 (VU0) on somatosensory cortex slices obtained
461 from Smo A1 rats at P14. VU0 application shifted the isoguvacine response from inhibitory to
462 excitatory when compared with non treated Smo A1 slices (-12 % vs +57.1% with VU0; p = 0.0009,
463 Mann-Whitney test; Fig. 3D) suggesting a KCC2-dependent mechanism for Smo-A1 action.

464 We next analyzed, using western blotting techniques, whether the expression of NKCC1 and
465 KCC2 protein levels were modified in Smo A1 and Smo Δ570-581 rats. We found that KCC2 protein

466 expression is up-regulated in Smo A1 electroporated cortices compared to Smo Δ570-581 (2.138 for
467 Smo A1 vs 1.98 Smo Δ570-581, when normalized to ß3 tubulin; $p = 0.0087$, Mann-Whitney test; Fig.
468 3E and F). No significant difference is observed between control and Smo-related constructs for
469 KCC2 protein levels. NKCC1 protein expression levels is similar between Smo A1 and Smo Δ570-
470 581 when compared to control (2.095 for Smo A1 vs 2.136 for Smo Δ570-581 and 2.167 for control
471 tissues when normalized to ß3 tubulin; $p = 0.09$ and $p = 0.48$ respectively, Mann Whitney test; Fig. 3E
472 and G).

473 Collectively, our data suggest that increasing Smo activity prematurely shifts GABA polarity
474 from excitatory to inhibitory in a KCC2-dependent manner, while decreasing Smo activity delays that
475 shift.

476

477 ***Neuronal chloride homeostasis is altered in the cerebral cortex of Smo A1 and Smo Δ570-581 rats***

478 The developmental shift from excitatory to inhibitory action of GABAergic transmission is mainly
479 dependent on extrusion activity of KCC2 in neuronal cells (Medina et al., 2014). We therefore sought
480 to determine whether the intracellular concentration of chloride is altered in the somatosensory cortex
481 of Smo A1 and Smo Δ570-581 rats. To test this hypothesis, constructs encoding ratiometric Cl-sensor
482 plus mCherry (control) or Smo A1 or Smo Δ570-581 were electroporated *in utero* in rats at E15 (see
483 Methods for details; Fig. 4A). Transverse slices of electroporated somatosensory cortex were prepared
484 at postnatal days P10 and P30. Electroporated slices harbored hundreds of neurons expressing Cl^--
485 Sensor in cortical layers V/VI. Results show that bath application of isoguvacine (10 µM, 3 min) on
486 P10 Smo Δ570-581 and mCherry-control slices produces a uniform decrease of $R_{430/500}$ (indicated by
487 an arrowhead in Fig. 4B and by the negative value of ΔR/R in Fig. 4D), reflecting a chloride ion
488 extrusion characteristic of depolarizing action of GABA (median values: -0.04 a.u. for Smo Δ570-581
489 vs -0.09 a.u. for CTRL; $p = 0.17$, Mann Whitney test; Fig. 4B and D), whereas in Smo A1 slices,
490 isoguvacine triggers either an increase or a decrease of $R_{430/500}$ (+0.00 a.u. for Smo A1; $p = 0.005$
491 compared to CTRL, Mann Whitney test, Fig. 4B and D), a characteristic feature indicating that GABA
492 is switching from depolarizing to hyperpolarizing actions. In P30 control and Smo A1 slices,
493 isoguvacine produces a chloride influx (indicated by an arrow in Fig. 4C) as shown by the positive

494 value of ΔR/R (+0.22 a.u. for CTRL mCherry vs +0.26 a.u. for Smo A1; $p = 0.63$, Mann-Whitney test;
495 Fig. 4C and D), while Smo Δ570-581 slices show a slight increase of $R_{430/500}$ (+0.06 a.u.; $p = 0.002$
496 compared to CTRL and $p = 0.01$ compared to Smo A1; Fig. 4C and D), suggesting that the conversion
497 of GABA-induced depolarization into hyperpolarization is altered in Smo Δ570-581 condition.
498 Our data therefore suggest that KCC2 activity is upregulated in Smo A1 and downregulated in
499 Smo Δ570-581, leading to low or high intracellular chloride concentration, respectively.
500
501 ***SmoΔ570-581 rats display increased susceptibility to PTZ-induced seizures***
502 We next investigated whether overexpression of Smo mutants may influence the susceptibility to
503 seizures. Smo Δ570-581, Smo A1 and age-matched control rats (transfected with mCherry or GFP
504 alone) at P30 were intraperitoneally injected with subconvulsive doses of PTZ (25 mg/kg) every 10
505 min (see Figure 5A). PTZ is known to induce seizures by reducing the $GABA_A$ receptor-mediated
506 inhibition (Kliouevа et al., 2001). The susceptibility to PTZ is age-dependent and previous studies
507 found that the lowest threshold for major seizures can be observed during the first 2 postnatal weeks of
508 life and the highest at around P30 (Vernadakis and Woodbury, 1969; Kliouevа et al., 2001). These
509 results suggest that the vulnerability of the developing cerebral cortex to PTZ is correlated to the
510 maturation of GABAergic system. Injections of PTZ were continued every 10 min until each rat had
511 generated generalized tonic-clonic seizure. Seizure susceptibility and severity were quantified with the
512 canonical Racine's scale of seizure severity (Lüttjohann et al., 2009), including dose and latency to
513 onset of the first generalized tonic-clonic seizure. Generalized seizures in Smo Δ570-581 rats (n = 18
514 rats) occur at lower doses of PTZ (median values: 87.5 mg/kg compared with 100 mg/kg for both
515 control and Smo A1 rats; $p = 0.005$ and $p = 0.003$ respectively, Mann-Whitney test; Fig. 5C) with
516 shorter latencies than control and Smo A1 rats (30.83 min compared with 32.71 min in control and
517 32.69 min in Smo A1; $p = 0.041$ and $p = 0.024$ respectively;, Mann-Whitney test; Fig. 5B). No
518 significant difference is observed between control and Smo A1 rats in the latency (32.69 min
519 compared with 32.71 min in control; $p = 0.5158$; Fig. 5B) or cumulative dose of PTZ to induce tonic-
520 clonic seizures ($p = 0.501$; Fig. 5C).
521 Together, our results indicate that reduced-seizure threshold in Smo Δ570-581 rats could be due

522 to a downregulation of KCC2 triggered by the diminution of Smo signaling pathway.

523

524 **Smo signaling controls chloride homeostasis in vitro**

525 To further link Shh-PTCH-Smo signaling with the GABA polarity shift and neuronal chloride
526 homeostasis, we performed gramicidin-perforated patch-clamp technique to measure the $GABA_A$
527 reversal potential (E_{GABA}) on dissociated hippocampal cultures in immature neurons (9 DIV). We first
528 measured E_{GABA} in transfected neurons (9 DIV) expressing mCherry or KCC2-pH_{ext} (Fig. 6A, B). In
529 accordance with results obtained from a recent study (Friedel et al., 2017), E_{GABA} is much lower in
530 KCC2-pH_{ext} transfected neurons than in mCherry cells (median values: -86.25 mV vs -50.13 mV
531 respectively; $p < 0.0001$, Mann-Whitney test; Fig. 6A and B). These results validate the functional
532 expression of KCC2-pH_{ext} overexpressed in hippocampal neurons, mimicking KCC2 neuronal activity
533 at mature stages. The measurements of E_{GABA} in Smo A1 transfected neurons show a hyperpolarizing
534 shift of isoguvacine currents when compared to mCherry neurons (-61.63 mV in Smo A1vs -50.13 mV
535 in mCherry; $p = 0.008$, Mann-Whitney test; Fig. 6A and B). In contrast, among neurons
536 overexpressing KCC2-pH_{ext}, those co-transfected with Smo Δ570-581 show a depolarizing shift of
537 isoguvacine currents when compared to KCC2-pH_{ext}–cotransfected mCherry neurons (-53.1 mV in
538 Smo Δ570-581 vs -86.25 mV in CTRL; $p = 0.006$, Mann-Whitney test; Fig. 6A and B). Our findings
539 suggest that the constitutively active Smo A1 upregulates KCC2 activity shifting E_{GABA} towards
540 hyperpolarizing values in hippocampal neurons at 9 DIV, whereas expression of the dominant-
541 negative Smo Δ570-581 in KCC2-pH_{ext}–expressing neurons downregulates KCC2 activity shifting
542 E_{GABA} towards depolarizing values. These results fit with our *ex vivo* data showing an impaired
543 chloride homeostasis either at high intracellular chloride concentration condition for Smo A1, or at
544 low intracellular chloride concentration condition for Smo Δ570-581.

545

546 **The dominant-negative form of Smo affects the stability of KCC2 to the plasmalemmal surface**
547 **by promoting endocytosis**

548 Finally, we assessed whether Smo-related constructs are able to regulate KCC2 trafficking to the cell
549 surface. We therefore quantified KCC2 expression in different cell compartments of control and Smo-

550 related constructs in cultured hippocampal neurons, using a KCC2 construct tagged in an external loop
551 with a green fluorescent protein (KCC2-pH_{ext}) (Kahle et al., 2014). This construct allowed us to
552 visualize the total amount of KCC2-pH_{ext} expressed by neurons (F_t), the level of KCC2-pH_{ext} cell
553 surface expression (F_m) and the level of KCC2-pH_{ext} internalized (F_i) (Fig. 7A and B). As controls, we
554 used KCC2 mutant constructions to stay at the membrane (A/A KCC2 mutant), or to not be addressed
555 to neuronal membrane (ΔNTD-KCC2 mutant). (Friedel et al., 2017). As expected KCC2 membrane
556 pool is increased for A/A KCC2 mutant condition (median values were: 1.49 a.u. for A/A KCC2 vs
557 0.94 a.u. for CTRL; p=0.002, Mann Whitney test; Fig. 7B, E). About ΔNTD-KCC2 mutant, the
558 multistep immunolabeling protocol didn't detect membrane expression (0.008 a.u. for ΔNTD-KCC2
559 vs 0.94 a.u. for CTRL; p<0.0001, Mann-Whitney test; Fig. 7B, E) or internalization (0.09 a.u. for
560 ΔNTD-KCC2 vs 0.84 a.u. for CTRL; p<0.0001, Mann-Whitney test; Fig. 7B, D), confirming cell
561 membrane integrity during experiment. Results show no difference in total KCC2 expression F_t
562 between control and Smo-related constructs (0.95 for CTRL vs 1.06 for Smo A1 and 1.06 a.u for Smo
563 Δ570-581; p = 0.28 and p = 0.31 respectively, Mann Whitney test; Fig. 7B and C). No difference is
564 observed between control and Smo A1 neurons for KCC2-pH_{ext} membrane pool F_m (0.94 vs 0.80 a.u.;
565 p = 0.40, Mann-Whitney test; Fig. 7E) or KCC2-pH_{ext} internalization F_i (0.84 vs 1.00 a.u.; p = 0.15,
566 Fig. 7D). Neurons expressing Smo Δ570-581 show a decrease in KCC2 surface expression compared
567 to control neurons (0.57 vs 0.94 a.u. for CTRL; p = 0.009; Fig. 7E) whereas, a large increase was
568 observed for KCC2 internalized clusters (2.57 a.u. for Smo Δ570-581 vs 0.84 a.u. for control, and 1.00
569 a.u. for Smo A1; p < 0.0001 and p = 0.0002 respectively; Fig. 7D). Interestingly, single membrane
570 cluster size shows a decrease compared to control in Smo Δ570-581 but not in Smo A1 neuronal cells
571 (1.02 a.u. for CTRL vs 0.92 a.u. for Smo Δ570-581 vs 0.99 a.u. for Smo A1; p < 0.0001 and p = 0.47
572 respectively; Fig. 7B and F). These results suggest that Smo Δ570-581 is able to regulate KCC2
573 membrane stability with an increased endocytosis leading to a lower KCC2 activity. Altogether, these
574 data suggest that Smo Δ570-581 affects the density of KCC2 cell surface expression and its stability to
575 the plasmalemmal surface by increasing endocytosis.

576

577 **Discussion**

578 In the present study, we investigated the actions of Shh-Smo signaling pathway on GABAergic
579 transmission *in vivo* and *ex vivo* in the rat somatosensory cortex and *in vitro* in primary culture of
580 hippocampal neurons using dominant-negative and constitutively-active forms of Smo (Smo Δ570-
581 581 and Smo A1 respectively). We show that activation of Smo signaling in immature neurons at early
582 postnatal stages accelerates the process of GABAergic switch form depolarizing to hyperpolarizing
583 activity in a KCC2-dependent manner, leading to a low intracellular chloride concentration.
584 Conversely, Smo signaling blockade alters KCC2 function and membrane stability, weakening the
585 GABAergic inhibition on later stages of the development, resulting in an increase of seizure
586 susceptibility. These findings reveal an unexpected function of the G-protein-coupled receptor
587 Smoothened on chloride homeostasis regulation and, in particular, on the timing of the GABA shift
588 from depolarizing- to hyperpolarizing-response of the postnatal developing brain.

589 The postnatal developmental switch in GABA polarity is tightly regulated by the actions of
590 several peptides including neurotrophic factors (Kelsch et al., 2001; Aguado et al., 2003; Ludwig et
591 al., 2011; Riffault et al., 2018), hypothalamic neurohormones (Tyzio et al., 2006; Leonzino et al.,
592 2016; Spoljaric et al., 2017), central and peripheral hormones (Sawano et al., 2013; Dumon et al.,
593 2018). Hence, the precise timing of GABAergic polarity shift depends on the balance between factors
594 promoting or delaying the onset of GABAergic inhibitory transmission. It is noteworthy that these
595 factors are developmentally regulated and/or operates within specific time windows to control the
596 functional expression of KCC2 and associated chloride homeostasis and, consequently the postnatal
597 maturation of GABAergic transmission in the central nervous system. Interestingly, the excitatory
598 action of GABA at early stages of the development, coincide with the predominance of trophic factors
599 responsible for the inhibition of KCC2 expression and function, such the immature form of BDNF
600 (proBDNF) (Riffault et al., 2018) and the adipocyte hormone leptin (Dumon et al., 2018). These two
601 factors are expressed shortly after birth and surge during the first postnatal week in rodents
602 (Menshanov et al., 2015; Dumon et al., 2018). They have been shown to promote a low KCC2 protein
603 and mRNA expression levels and consequently a high intracellular chloride concentration, thus
604 maintaining a depolarizing action of GABA in neonates. The developmental decreases of leptin and
605 proBDNF observed at the end of the first postnatal week in rodents, are concomitant to an increase in

606 oxytocin (Tyzio et al., 2006; Leonzino et al., 2016), mature BDNF (mBDNF) (Maisonpierre et al.,
607 1990) and thyroid hormones (Sawano et al., 2013), which in turn, up-regulates KCC2, leading to a low
608 intracellular chloride and a hyperpolarizing action of GABA. During the postnatal developmental
609 period, Shh expression paralleled the temporal expression of mBDNF in the rodents cortex with a
610 nearly undetectable level at birth and a continuous increased expression at both mRNA and protein
611 levels during the first postnatal weeks (Rivell et al., 2019). This temporal expression of Shh and its
612 signaling partners during postnatal brain development has been shown to play a role in neuronal
613 network construction through axonal growth and synaptic maturation (Yao et al., 2015). Here, we
614 uncover a new critical function of Shh components in the regulation of the GABA polarity switch.
615 Indeed, we showed that activation of the $GABA_A$ receptor by isoguvacine, in immature (i.e. post-natal
616 day 14) Smo A1 cortical neurons results in an influx of chloride and a decrease in spiking activity
617 whereas, in mature (i.e. post-natal day 30) dominant negative Smo cortical neurons (Smo Δ570-581),
618 maintains a depolarizing and excitatory action of GABA. Thus in the absence of Smo signaling, the
619 GABA shift is delayed, thereby leading to an altered chloride homeostasis and higher susceptibility to
620 seizures, presumably reflecting an unbalanced excitation to inhibition (E/I) ratio. E/I imbalance has
621 been linked to cognitive disorders such as schizophrenia, autism spectrum disorders (ASD),
622 depression and epilepsy (Brambilla et al., 2003; Ben-Ari and Holmes, 2005; Kuzirian and Paradis,
623 2011; Mueller et al., 2015). Abnormal levels of Shh have been also observed in ASD patients with
624 either an increased serum level in children or a decreased mRNA level in post-mortem adult human
625 brain tissue from autism patients (Choi et al., 2014; Halepoto et al., 2015). In addition, mutations in
626 PTCHD1, a gene displaying secondary structures similar to PTCH1, are found in patients with
627 intellectual disability and ASD (Ung et al., 2018). Consistent with a possible role of Shh components
628 in the regulation of the E/I balance, these observations also suggest that an alteration in Shh-PTCH-
629 Smo pathway may have an implication to the pathophysiological mechanisms in ASD. In line with
630 these observations, the role of Shh signaling in neuronal activity has been recently addressed in an
631 elegant study (Hill et al., 2019) showing that the selective disruption of Shh signaling with a
632 conditional knockout of Smo leads to an increase in neuronal excitability of cortical neurons, thus
633 highlighting the importance of Shh on the E/I equilibrium and the construction of functional cortical

634 networks. The results from this study are consistent with our findings from, showing that Shh
635 signaling blockade increases neuronal network excitability in rodents expressing the dominant
636 negative form of Smo. Furthermore, our *in vivo* experiments indicate that the threshold for PTZ-
637 induced tonic-clonic seizure was reduced in Smo Δ570-581 rodents. The implication of Shh signaling
638 in epilepsy and seizures has been indirectly addressed in previous studies showing that somatic
639 mutations in Shh pathway genes in human are associated with hypothalamic hamartoma and drug-
640 resistant epilepsy (Hildebrand et al., 2016; Saitsu et al., 2016). Likewise, the Shh expression was
641 increased in hippocampus and neocortex from both human and animal models of temporal lobe
642 epilepsy (TLE) (Fang et al., 2011), thus suggesting a potential relationship between epilepsy and Shh
643 activity. In line of the above studies, Feng et al. (Feng et al., 2016) reported that during TLE
644 development, Shh contributes to epileptogenesis through the inhibition of glutamate transporters
645 function leading to abnormal extracellular glutamate levels, whereas the blockade of Shh signaling
646 pathway reduced the severity of seizures. Together, these observations can lead to opposing
647 interpretations regarding the possible interplay between Shh pathway and epilepsy. These apparent
648 discrepancies could be explained by the treatments utilized (i.e. acute seizure models with PTZ versus
649 spontaneous seizures in the pilocarpine model of chronic TLE) that are able to activate different
650 downstream signaling cascades (Choudhry et al., 2014). Moreover, other studies have found that the
651 Shh/Gli pathway activation increased the synthesis and secretion of neurotrophic factors like nerve
652 growth factor (NGF) and BDNF (Radzikinas et al., 2011; Bond et al., 2013; Chen et al., 2018), which
653 they may have neuroprotective effects in TLE (Paradiso et al., 2009; Bovolenta et al., 2010; Falcicchia
654 et al., 2018). Clearly, additional studies are needed to get a deeper knowledge on the cellular and
655 molecular mechanisms linking epilepsy to Shh pathway components.

656 Importantly, our *in vitro* experiments revealed that the reversal potential of GABA responses
657 (E_{GABA}) shifted towards a more hyperpolarized level in Smo A1 expressing neurons and conversely
658 towards more depolarized values in Smo Δ570-581 neurons. It is well known that these changes in
659 E_{GABA} values are also closely related to the functional expression of KCC2 (Rivera et al., 1999). KCC2
660 activity levels are determined by its cell surface targeting and clustering (Medina et al., 2014; Côme et
661 al., 2019a). Thus, KCC2 cycle between synaptic sites and endocytic compartments which depends on

662 the phosphorylation and/or dephosphorylation state on different amino-acid residues (Kahle et al.,
663 2014; Kahle and Delpire, 2016; Côme et al., 2019), but also this membrane turnover requires
664 regulation to its cytosolic N- and C-termini (Friedel et al., 2017). For instance, N-terminal truncation
665 of KCC2 prevents its export at the cell surface, whereas C-terminal truncation leads to a decreased
666 surface expression of KCC2 (Friedel et al., 2017). The observed loss of KCC2 surface expression in
667 the C-terminal mutants mice is explained by an increase in the internalization rate without affecting
668 cell surface delivery. Furthermore, KCC2 function can also be regulated through lateral diffusion at
669 the plasma membrane (Chamma et al., 2013). This suggest that KCC2 membrane dispersion may, in
670 turn, mediates membrane destabilization and endocytosis resulting in intracellular chloride
671 homeostatic dysregulation (Côme et al., 2019). In agreement with this, we found that inhibition of
672 Smo signaling pathway in mature neurons induces a decreases in KCC2 cluster size and enhances the
673 intracellular concentration of chloride that sets E_{GABA} at more positive values than the resting potential
674 with a reduced plasmalemmal levels of KCC2 cell surface expression levels. We further show that
675 these effects occur through an increased rate of KCC2 turnover.

676 In conclusion, these data uncovering an unexpected role of Shh components during early
677 postnatal development in the regulation of the E/I balance through the control of chloride homeostasis.
678 Thus Shh signaling will tune up or down GABA inhibitory transmission by acting on chloride
679 homeostasis and trafficking of KCC2 at the cell membrane. Although the molecular links between Shh
680 and KCC2 require further studies, our observations suggest that Shh is able to set the cursor of
681 GABAergic inhibitory switch during this critical maturational period where developmental
682 pathogenesis takes place.

683 **References**

684 Aguado F, Carmona MA, Pozas E, Aguiló A, Martínez-Guijarro FJ, Alcantara S, Borrell V, Yuste R,
685 Ibañez CF, Soriano E (2003) BDNF regulates spontaneous correlated activity at early developmental
686 stages by increasing synaptogenesis and expression of the K+/Cl- co-transporter KCC2. *Dev Camb*
687 *Engl* 130:1267–1280.

688 Al-Ayadhi LY (2012) Relationship Between Sonic Hedgehog Protein, Brain-Derived Neurotrophic
689 Factor and Oxidative Stress in Autism Spectrum Disorders. *Neurochem Res* 37:394–400.

690 Álvarez-Buylla A, Ihrie RA (2014) Sonic Hedgehog Signaling in the Postnatal Brain. *Semin Cell Dev*
691 *Biol* 0:105–111.

692 Antonelli F, Casciati A, Pazzaglia S (2019) Sonic hedgehog signaling controls dentate gyrus
693 patterning and adult neurogenesis in the hippocampus. *Neural Regen Res* 14:59–61.

694 Araújo GL, Araújo JA, Schroeder T, Tort AB, Costa MR (2014) Sonic hedgehog signaling regulates
695 mode of cell division of early cerebral cortex progenitors and increases astrogliogenesis. *Front Cell*
696 *Neurosci* 8.

697 Belgacem YH, Borodinsky LN (2015) Inversion of Sonic hedgehog action on its canonical pathway
698 by electrical activity. *Proc Natl Acad Sci USA* 112:4140–4145.

699 Belgacem YH, Hamilton AM, Shim S, Spencer KA, Borodinsky LN (2016) The Many Hats of Sonic
700 Hedgehog Signaling in Nervous System Development and Disease. *J Dev Biol* 4.

701 Ben-Ari Y (2002) Excitatory actions of gaba during development: the nature of the nurture. *Nat Rev*
702 *Neurosci* 3:728–739.

703 Ben-Ari Y, Cherubini E, Corradetti R, Gaiarsa JL (1989) Giant synaptic potentials in immature rat
704 CA3 hippocampal neurones. *J Physiol* 416:303–325.

705 Ben-Ari Y, Gaiarsa J-L, Tyzio R, Khazipov R (2007) GABA: a pioneer transmitter that excites
706 immature neurons and generates primitive oscillations. *Physiol Rev* 87:1215–1284.

707 Ben-Ari Y, Holmes GL (2005) The multiple facets of gamma-aminobutyric acid dysfunction in
708 epilepsy. *Curr Opin Neurol* 18:141–145.

709 Beug ST, Parks RJ, McBride HM, Wallace VA (2011) Processing-dependent trafficking of Sonic
710 hedgehog to the regulated secretory pathway in neurons. *Mol Cell Neurosci* 46:583–596.

711 Bezard E, Baufreton J, Owens G, Crossman AR, Dudek H, Taupignon A, Brotchie JM. 2003. Sonic
712 hedgehog is a neuromodulator in the adult subthalamic nucleus. *FASEB J* 17:2337–2338.
713 Bond CW, Angeloni N, Harrington D, Stupp S, Podlasek CA (2013) Sonic Hedgehog regulates brain-
714 derived neurotrophic factor in normal and regenerating cavernous nerves. *J Sex Med* 10:730–737.
715 Bovolenta R, Zucchini S, Paradiso B, Rodi D, Merigo F, Navarro Mora G, Osculati F, Berto E,
716 Marconi P, Marzola A, Fabene PF, Simonato M (2010) Hippocampal FGF-2 and BDNF
717 overexpression attenuates epileptogenesis-associated neuroinflammation and reduces spontaneous
718 recurrent seizures. *J Neuroinflammation* 7:81.
719 Breunig JJ, Sarkisian MR, Arellano JI, Morozov YM, Ayoub AE, Sojitra S, Wang B, Flavell RA,
720 Rakic P, Town T (2008) Primary cilia regulate hippocampal neurogenesis by mediating sonic
721 hedgehog signaling. *Proc Natl Acad Sci U S A* 105:13127–13132.
722 Briscoe J, Thérond PP (2013) The mechanisms of Hedgehog signalling and its roles in development
723 and disease. *Nat Rev Mol Cell Biol* 14:416–429.
724 Buerli T, Pellegrino C, Baer K, Lardi-Studler B, Chudotvorova I, Fritschy J-M, Medina I, Fuhrer C
725 (2007) Efficient transfection of DNA or shRNA vectors into neurons using magnetofection. *Nat*
726 *Protoc* 2:3090–3101.
727 Chamma I, Heubl M, Chevy Q, Renner M, Moutkine I, Eugène E, Poncer JC, Lévi S (2013) Activity-
728 Dependent Regulation of the K/Cl Transporter KCC2 Membrane Diffusion, Clustering, and Function
729 in Hippocampal Neurons. *J Neurosci* 33:15488–15503.
730 Charytoniuk D, Porcel B, Rodríguez Gomez J, Faure H, Ruat M, Traiffort E (2002) Sonic Hedgehog
731 signalling in the developing and adult brain. *J Physiol* (Paris) 96:9–16.
732 Chen S-D, Yang J-L, Hwang W-C, Yang D-I (2018) Emerging Roles of Sonic Hedgehog in Adult
733 Neurological Diseases: Neurogenesis and Beyond. *Int J Mol Sci* 19.
734 Chen Y, Sasai N, Ma G, Yue T, Jia J, Briscoe J, Jiang J (2011) Sonic Hedgehog dependent
735 phosphorylation by CK1α and GRK2 is required for ciliary accumulation and activation of
736 smoothened. *PLoS Biol* 9:e1001083.
737 Choi J, Ababon MR, Soliman M, Lin Y, Brzustowicz LM, Matteson PG, Millonig JH (2014) Autism
738 associated gene, engrailed2, and flanking gene levels are altered in post-mortem cerebellum. *PloS One*

739 9:e87208.
740 Choudhry Z, Rikani AA, Choudhry AM, Tariq S, Zakaria F, Asghar MW, Sarfraz MK, Haider K,
741 Shafiq AA, Mobassarah NJ (2014) Sonic hedgehog signalling pathway: a complex network. *Ann*
742 *Neurosci* 21:28–31.
743 Côme E, Heubl M, Schwartz EJ, Poncer JC, Lévi S (2019) Reciprocal Regulation of KCC2
744 Trafficking and Synaptic Activity. *Front Cell Neurosci* 13.
745 Dumon C, Diabira D, Chudotvorova I, Bader F, Sahin S, Zhang J, Porcher C, Wayman G, Medina I,
746 Gaiarsa J-L (2018) The adipocyte hormone leptin sets the emergence of hippocampal inhibition in
747 mice. *eLife* 7.
748 Falcicchia C, Paolone G, Emerich DF, Lovisari F, Bell WJ, Fradet T, Wahlberg LU, Simonato M
749 (2018) Seizure-Suppressant and Neuroprotective Effects of Encapsulated BDNF-Producing Cells in a
750 Rat Model of Temporal Lobe Epilepsy. *Mol Ther Methods Clin Dev* 9:211–224.
751 Fang M, Lu Y, Chen G-J, Shen L, Pan Y-M, Wang X-F (2011) Increased expression of Sonic
752 hedgehog in temporal lobe epileptic foci in humans and experimental rats. *Neuroscience* 182:62–70.
753 Feng S, Ma S, Jia C, Su Y, Yang S, Zhou K, Liu Y, Cheng J, Lu D, Fan L, Wang Y (2016) Sonic
754 hedgehog is a regulator of extracellular glutamate levels and epilepsy. *EMBO Rep* 17:682–694.
755 Friedel P, Bregestovski P, Medina I (2013) Improved method for efficient imaging of intracellular Cl(-
756) with Cl-Sensor using conventional fluorescence setup. *Front Mol Neurosci* 6:7.
757 Friedel P, Kahle KT, Zhang J, Hertz N, Pisella LI, Buhler E, Schaller F, Duan J, Khanna AR, Bishop
758 PN, Shokat KM, Medina I (2015) WNK1-regulated inhibitory phosphorylation of the KCC2
759 cotransporter maintains the depolarizing action of GABA in immature neurons. *Sci Signal* 8:ra65–
760 ra65.
761 Friedel P, Ludwig A, Pellegrino C, Agez M, Jawhari A, Rivera C, Medina I (2017) A Novel View on
762 the Role of Intracellular Tails in Surface Delivery of the Potassium-Chloride Cotransporter KCC2.
763 *eNeuro* 4.
764 Halepoto DM, Bashir S, Zeina R, Al-Ayadhi LY (2015) Correlation Between Hedgehog (Hh) Protein
765 Family and Brain-Derived Neurotrophic Factor (BDNF) in Autism Spectrum Disorder (ASD). *J Coll*
766 *Physicians Surg Pak* 25:882–885.

767 Hammond R, Blaess S, Abeliovich A (2009) Sonic Hedgehog Is a Chemoattractant for Midbrain
768 Dopaminergic Axons. *PLOS ONE* 4:e7007.
769 Harwell CC, Parker PRL, Gee SM, Okada A, McConnell SK, Kreitzer AC, Kriegstein AR (2012)
770 Sonic hedgehog expression in corticofugal projection neurons directs cortical microcircuit formation.
771 *Neuron* 73:1116–1126.
772 Hildebrand MS, Griffin NG, Damiano JA, Cops EJ, Burgess R, Ozturk E, Jones NC, Leventer RJ,
773 Freeman JL, Harvey AS, Sadleir LG, Scheffer IE, Major H, Darbro BW, Allen AS, Goldstein DB,
774 Kerrigan JF, Berkovic SF, Heinzen EL (2016) Mutations of the Sonic Hedgehog Pathway Underlie
775 Hypothalamic Hamartoma with Gelastic Epilepsy. *Am J Hum Genet* 99:423–429.
776 Hill SA, Blaeser AS, Coley AA, Xie Y, Shepard KA, Harwell CC, Gao W-J, Garcia ADR (2019)
777 Sonic hedgehog signaling in astrocytes mediates cell-type-specific synaptic organization. *eLife* 8.
778 Jacob L, Lum L (2007) Deconstructing the Hedgehog Pathway in Development and Disease. *Science*
779 318:66–68.
780 Jeong J, Mao J, Tenzen T, Kottmann AH, McMahon AP (2004) Hedgehog signaling in the neural
781 crest cells regulates the patterning and growth of facial primordia. *Genes Dev* 18:937–951.
782 Kahle KT, Delpire E. 2016. Kinase-KCC2 coupling: Cl- rheostasis, disease susceptibility, therapeutic
783 target. *J Neurophysiol* 115:8–18.
784 Kahle KT et al. (2014) Genetically encoded impairment of neuronal KCC2 cotransporter function in
785 human idiopathic generalized epilepsy. *EMBO Rep* 15:766–774.
786 Kelsch W, Hormuzdi S, Straube E, Lewen A, Monyer H, Misgeld U (2001) Insulin-like growth factor
787 1 and a cytosolic tyrosine kinase activate chloride outward transport during maturation of hippocampal
788 neurons. *J Neurosci* 21:8339–8347.
789 Khazipov R, Zaynutdinova D, Ogievetsky E, Valeeva G, Mitrukhina O, Manent J-B, Represa A
790 (2015) Atlas of the Postnatal Rat Brain in Stereotaxic Coordinates. *Front Neuroanat* 9.
791 Kilb W, Kirischuk S, Luhmann HJ (2013) Role of tonic GABAergic currents during pre- and early
792 postnatal rodent development. *Front Neural Circuits* 7.
793 Kim J, Kato M, Beachy PA (2009) Gli2 trafficking links Hedgehog-dependent activation of
794 Smoothened in the primary cilium to transcriptional activation in the nucleus. *Proc Natl Acad Sci U S*

795 *A* 106:21666–21671.
796 Kirmse K, Kummer M, Kovalchuk Y, Witte OW, Garaschuk O, Holthoff K (2015) GABA depolarizes
797 immature neurons and inhibits network activity in the neonatal neocortex in vivo. *Nat Commun*
798 6:7750.
799 Kliouevа IA, van Luijtelaar EL, Chepurnova NE, Chepurnov SA (2001) PTZ-induced seizures in rats:
800 effects of age and strain. *Physiol Behav* 72:421–426.
801 Kriegstein AR, Noctor SC (2004) Patterns of neuronal migration in the embryonic cortex. *Trends*
802 *Neurosci* 27:392–399.
803 Krogsgaard-Larsen P, Johnston G a. R (1978) Structure-Activity Studies on the Inhibition of Gaba
804 Binding to Rat Brain Membranes by Muscimol and Related Compounds. *J Neurochem* 30:1377–1382.
805 Kuzirian MS, Paradis S (2011) Emerging themes in GABAergic synapse development. *Prog*
806 *Neurobiol* 95:68–87.
807 Leonzino M, Busnelli M, Antonucci F, Verderio C, Mazzanti M, Chini B (2016) The Timing of the
808 Excitatory-to-Inhibitory GABA Switch Is Regulated by the Oxytocin Receptor via KCC2. *Cell Rep*
809 15:96–103.
810 Logue SE, Martin SJ (2008) Caspase activation cascades in apoptosis. *Biochem Soc Trans* 36:1–9.
811 Ludwig A, Uvarov P, Soni S, Thomas-Crusells J, Airaksinen MS, Rivera C (2011) Early growth
812 response 4 mediates BDNF induction of potassium chloride cotransporter 2 transcription. *J Neurosci*
813 31:644–649.
814 Lüttjohann A, Fabene PF, van Luijtelaar G (2009) A revised Racine's scale for PTZ-induced seizures
815 in rats. *Physiol Behav* 98:579–586.
816 Maisonpierre PC, Belluscio L, Friedman B, Alderson RF, Wiegand SJ, Furth ME, Lindsay RM,
817 Yancopoulos GD (1990) NT-3, BDNF, and NGF in the developing rat nervous system: parallel as well
818 as reciprocal patterns of expression. *Neuron* 5:501–509.
819 Markova O, Mukhtarov M, Real E, Jacob Y, Bregestovski P (2008) Genetically encoded chloride
820 indicator with improved sensitivity. *J Neurosci Methods* 170:67–76.
821 Martineau FS, Sahu S, Plantier V, Buhler E, Schaller F, Fournier L, Chazal G, Kawasaki H, Represa
822 A, Watrin F, Manent J-B (2018) Correct Laminar Positioning in the Neocortex Influences Proper

823 Dendritic and Synaptic Development. *Cereb Cortex* 28:2976–2990.

824 Medina I, Friedel P, Rivera C, Kahle KT, Kourdougli N, Uvarov P, Pellegrino C (2014) Current view
825 on the functional regulation of the neuronal K(+)-Cl(-) cotransporter KCC2. *Front Cell Neurosci* 8:27.

826 Memi F, Zecevic N, Radonjić N (2018) Multiple roles of Sonic Hedgehog in the developing human
827 cortex are suggested by its widespread distribution. *Brain Struct Funct* 223:2361–2375.

828 Menshanov PN, Lanshakov DA, Dygalo NN (2015) proBDNF is a major product of bdnf gene
829 expressed in the perinatal rat cortex. *Physiol Res Acad Sci Bohemoslov* 64:925-934.

830 Mitchell N, Petralia RS, Currier DG, Wang Y-X, Kim A, Mattson MP, Yao PJ (2012) Sonic hedgehog
831 regulates presynaptic terminal size, ultrastructure and function in hippocampal neurons. *J Cell Sci*
832 125:4207–4213.

833 Mueller TM, Remedies CE, Haroutunian V, Meador-Woodruff JH (2015) Abnormal subcellular
834 localization of GABAA receptor subunits in schizophrenia brain. *Transl Psychiatry* 5:e612.

835 Paradiso B, Marconi P, Zucchini S, Berto E, Binaschi A, Bozac A, Buzzi A, Mazzuferi M, Magri E,
836 Navarro Mora G, Rodi D, Su T, Volpi I, Zanetti L, Marzola A, Manservigi R, Fabene PF, Simonato M
837 (2009) Localized delivery of fibroblast growth factor-2 and brain-derived neurotrophic factor reduces
838 spontaneous seizures in an epilepsy model. *Proc Natl Acad Sci U S A* 106:7191–7196.

839 Parra LM, Zou Y (2010) Sonic hedgehog induces response of commissural axons to Semaphorin
840 repulsion during midline crossing. *Nat Neurosci* 13:29–35.

841 Pascual O, Traiffort E, Baker DP, Galdes A, Ruat M, Champagnat J (2005) Sonic hedgehog signalling
842 in neurons of adult ventrolateral nucleus tractus solitarius. *Eur J Neurosci* 22:389–396.

843 Paxinos G, Watson C (2005) The Rat Brain in Stereotaxic Coordinates. Elsevier Academic Press

844 Petralia RS, Schwartz CM, Wang Y-X, Mattson MP, Yao PJ (2011) Subcellular localization of
845 Patched and Smoothened, the receptors for Sonic hedgehog signaling, in the hippocampal neuron. *J*
846 *Comp Neurol* 519:3684–3699.

847 Petralia RS, Wang Y-X, Mattson MP, Yao PJ (2012) Subcellular distribution of patched and
848 smoothened in the cerebellar neurons. *Cerebellum Lond Engl* 11:972–981.

849 Qin, Suping. 2019. Downregulation of sonic hedgehog signaling in the hippocampus leads to neuronal
850 apoptosis in high-fat diet-fed mice. *Behav Brain Res* 367:91-100.

851 Radzikinas K, Aven L, Jiang Z, Tran T, Paez-Cortez J, Boppidi K, Lu J, Fine A, Ai X (2011) A
852 Shh/miR-206/BDNF Cascade Coordinates Innervation and Formation of Airway Smooth Muscle. *J*
853 *Neurosci* 31:15407–15415.
854 Riffault B, Kourdougli N, Dumon C, Ferrand N, Buhler E, Schaller F, Chambon C, Rivera C, Gaiarsa
855 J-L, Porcher C (2018) Pro-Brain-Derived Neurotrophic Factor (proBDNF)-Mediated p75NTR
856 Activation Promotes Depolarizing Actions of GABA and Increases Susceptibility to Epileptic
857 Seizures. *Cereb Cortex* 28:510-527.
858 Riobo NA, Saucy B, Dilizio C, Manning DR (2006) Activation of heterotrimeric G proteins by
859 Smoothened. *Proc Natl Acad Sci U S A* 103:12607–12612.
860 Rivell A, Petralia RS, Wang Y-X, Clawson E, Moehl K, Mattson MP, Yao PJ (2019) Sonic hedgehog
861 expression in the postnatal brain. *Biol Open* 8.
862 Rivera C, Voipio J, Payne JA, Ruusuvuori E, Lahtinen H, Lamsa K, Pirvola U, Saarma M, Kaila K
863 (1999) The K+/Cl- co-transporter KCC2 renders GABA hyperpolarizing during neuronal maturation.
864 *Nature* 397:251–255.
865 Ruat M, Roudaut H, Ferent J, Traiffort E (2012) Hedgehog trafficking, cilia and brain functions.
866 *Differ Res Biol Divers* 83:S97-104.
867 Saitsu H, Sonoda M, Higashijima T, Shirozu H, Masuda H, Tohyama J, Kato M, Nakashima M,
868 Tsurusaki Y, Mizuguchi T, Miyatake S, Miyake N, Kameyama S, Matsumoto N (2016) Somatic
869 mutations in GLI3 and OFD1 involved in sonic hedgehog signaling cause hypothalamic hamartoma.
870 *Ann Clin Transl Neurol* 3:356–365.
871 Sawano E, Takahashi M, Negishi T, Tashiro T (2013) Thyroid hormone-dependent development of
872 the GABAergic pre- and post-synaptic components in the rat hippocampus. *Int J Dev Neurosci Off J*
873 *Int Soc Dev Neurosci* 31:751–761.
874 Sernagor E (2010) GABAergic control of neurite outgrowth and remodeling during development and
875 adult neurogenesis: general rules and differences in diverse systems. *Front Cell Neurosci* 4.
876 Spoljaric A, Seja P, Spoljaric I, Virtanen MA, Lindfors J, Uvarov P, Summanen M, Crow AK, Hsueh
877 B, Puskarjov M, Ruusuvuori E, Voipio J, Deisseroth K, Kaila K (2017) Vasopressin excites
878 interneurons to suppress hippocampal network activity across a broad span of brain maturity at birth.

879 *Proc Natl Acad Sci U S A* 114:E10819–E10828.

880 Su Y, Yuan Y, Feng S, Ma S, Wang Y (2017) High frequency stimulation induces sonic hedgehog
881 release from hippocampal neurons. *Sci Rep* 7:43865.

882 Traiffort E, Angot E, Ruat M (2010) Sonic Hedgehog signaling in the mammalian brain. *J Neurochem*
883 113:576–590.

884 Tyzio R, Cossart R, Khalilov I, Minlebaev M, Hübner CA, Represa A, Ben-Ari Y, Khazipov R (2006)
885 Maternal oxytocin triggers a transient inhibitory switch in GABA signaling in the fetal brain during
886 delivery. *Science* 314:1788–1792.

887 Ung DC et al. (2018) Ptchd1 deficiency induces excitatory synaptic and cognitive dysfunctions in
888 mouse. *Mol Psychiatry* 23:1356–1367.

889 Vernadakis A, Woodbury DM (1969) The developing animal as a model. *Epilepsia* 10:163–178.

890 Wang B, Zhang Y, Dong H, Gong S, Wei B, Luo M, Wang H, Wu X, Liu W, Xu X, Zheng Y, Sun M
891 (2018) Loss of Tctn3 causes neuronal apoptosis and neural tube defects in mice. *Cell Death Dis* 9:520.

892 Wang DD, Kriegstein AR (2009) Defining the role of GABA in cortical development. *J Physiol*
893 587:1873–1879.

894 Waseem T, Mukhtarov M, Buldakova S, Medina I, Bregestovski P (2010) Genetically encoded Cl-
895 Sensor as a tool for monitoring of Cl-dependent processes in small neuronal compartments. *J Neurosci*
896 *Methods* 193:14–23.

897 Wu C, Sun D (2015) GABA receptors in brain development, function, and injury. *Metab Brain Dis*
898 30:367–379.

899 Yao PJ, Petralia RS, Mattson MP (2016) Sonic Hedgehog Signaling and Hippocampal
900 Neuroplasticity. *Trends Neurosci* 39:840–850.

901 Yao PJ, Petralia RS, Ott C, Wang Y-X, Lippincott-Schwartz J, Mattson MP (2015) Dendrosomatic
902 Sonic Hedgehog Signaling in Hippocampal Neurons Regulates Axon Elongation. *J Neurosci*
903 35:16126–16141.

904 Zhang XM, Ramalho-Santos M, McMahon AP (2001) Smoothened mutants reveal redundant roles for
905 Shh and Ihh signaling including regulation of L/R asymmetry by the mouse node. *Cell* 105:781–792.

906 Zuñiga NR, Stoeckli ET (2017) Sonic Hedgehog—'Jack-of-All-Trades' in Neural Circuit Formation. *J*

Dev Biol 5:2.

911 **Figure Legends**

912 **Figure 1: Cortical expression pattern of Smo-related constructs.** (A) Representative neocortical
913 section showing laminar position of transfected cells electroporated at E15 with control GFP alone
914 (CTRL – GFP) or co-electroporated with Smo A1 (SmoA1 – GFP) or Smo Δ570-587 (Smo Δ570-587
915 – GFP) and processed postnatally at P15 and co-immunostained with NeuN (blue) and FoxP2 (red).
916 GFP fluorescence intensity profile shows that E15 generated neurons are distributed mainly in deeper
917 layers V-VI. Scale bar = 250 µm. (B) Box plots of cortical thickness in GFP control (CTRL), Smo A1
918 and Smo Δ570-587 brains. Mann-Whitney test. (C) Boxplot of neuronal density in GFP control, Smo
919 A1 and Smo Δ570-587 brains. Mann-Whitney test. (D) Box plots of neurons soma size on P15
920 electroporated rats. Mann-Whitney test. (E) Box plots of synaptophysin area fraction normalized with
921 MAP2 area fraction (left; Mann-Whitney test) and (right) example of immunofluorescence signal of
922 P30 cortical section expressing Smo Δ570-581 - GFP, co-immunostained with Synaptophysin (red)
923 and MAP2 (blue). Scale bar = 30 µm. (F) Immunofluorescence signal of P15 cortical sections
924 electroporated at E15 with GFP (CTRL – GFP) with or without Smo-related constructs and
925 immunolabeled with cleaved caspase-3 antibody. Scale bar = 100 µm. (G) Ratio of cleaved caspase-3-
926 positive neurons (apoptotic) per surface area and expressed as a percentage of control (GFP).
927 Overexpression of Smo A1 or Smo Δ570-581 does not increase the number of apoptotic neurons
928 compared to control (GFP). Mann-Whitney test. Errors bars are mean ± SD. Number of slices and rats
929 are indicated in parenthesis. *$p < 0.05$; **$p < 0.01$; **$p < 0.001$.

930

931 **Figure 2: Smo-related constructs regulate the expression levels of PTCH1 and Gli1.** (A) Cells
932 overexpressing Smo related constructs (green) and immunostained with Smo antibody (red) showed a
933 similar localization (overlay). Scale bar = 25 µm. (B and C) Box plots of relative expression of Gli1
934 and PTCH1 mRNA transcripts in GFP (CTRL), SmoA1 and Smo Δ570-581 rats. (B) Box plots of Gli1
935 and (C) PTCH1 genes expression are normalized to GAPDH expression in the same RNA preparation.
936 Scale bar = 25 µm. n=6 rats for each condition. Mann-Whitney test. *$p > 0.05$; ** $p < 0.01$.

937

938 **Figure 3: The developmental shift in the polarity of $GABA_AR$ mediated responses is modulated**

939 **in cortical neurons expressing the dominant negative or the constitutively active forms of Smo**.
940 (A) Effects of isoguvacine (10 µM) in cortical slices from control GFP, Smo A1 and Smo Δ570-581
941 rats: representative traces of spontaneous extracellular field potentials (left column) recorded in
942 electroporated area of cortical slices at P14 in GFP (CTRL) and Smo A1 and at P30 in CTRL and Smo
943 Δ570-581 rats (left column). Corresponding time course of normalized frequency MUA is shown
944 beside (right column) (B) Box plots of relative change of isoguvacine-dependent MUA frequency in
945 electroporated rats at P14, P20 and P30. Numbers in parenthesis indicate the number of slices recorded
946 and rats used. (C) Developmental regulation of GABAergic excitation in electroporated rats.
947 Proportion of excited slices is the proportion of slices showing an increase of 20% or more of MUA
948 frequency during isoguvacine application. (D) Box plots of relative changes in MUA frequency during
949 isoguvacine application with and without VU0463271 (VU0) a KCC2-selective blocker application on
950 Smo A1 rats at P14. Mann-Whitney test. (E) Immunoblots for NKCC1 and KCC2 protein extracts
951 from GFP, Smo A1 and Smo Δ570-581 electroporated somatosensory cortices. (F and G) Box plots of
952 normalized KCC2 and NKCC1 relative protein level. n=6 rats for each condition. Mann-Whitney test.
953 *$p < 0.05$; ** $p < 0.01$; ***$p < 0.001$.
954
955 **Figure 4: Smo-dependent regulation of Cl-Sensor ratiometric fluorescence in acute cortical slices**
956 **prepared from rats on P10 and P30**. Rats were electroporated *in utero* at embryonic day 15 with Cl-
957 Sensor plus mCherry (CTRL) or Cl-Sensor plus Smo A1 (Smo A1) or Cl-Sensor plus Smo Δ570-581
958 (Smo Δ570-581). Data represent results obtained from 4-5 rats per experimental condition and 1-2
959 slices were recorded per animal. (A) Typical images of Cl-Sensor fluorescence excited at 500nm in
960 slice from P30 rat electroporated with Cl- Sensor plus Smo A1. The region of interest is drawn around
961 the soma of cells located in the focal plane. (B and C) Example of typical ratiometric fluorescence
962 (R430/500) recordings at P10 and P30 from control (CTRL), Smo A1 and Smo Δ570-581 rats.
963 Horizontal bars indicate the times of application of ACSF containing isoguvacine. Arrows and
964 arrowheads indicate different types of responses between control, Smo A1 and Smo Δ570-581 neurons
965 at P10 and P30. (D) Box plots quantification of fluorescence change of ΔR/R, where R is the mean of
966 5 measurements before isoguvacine application and ΔR is the difference between absolute maximum

967 of isoguvacine-induced response. Number of slices and rats are indicated in parenthesis. *$p < 0.01$,
968 **$p < 0.01$ when compared to control at the same age. Mann-Whitney test.
969
970 **Figure 5: Modified susceptibility to pentylenetrazol-induced (PTZ) seizures in Smo mutant rats**.
971 (A) Experimental paradigm design. (B) Boxplot of latency needed to induce generalized tonic-clonic
972 seizures in 3 groups of electroporated rats: control (CTR; electroporated with mCherry or GFP), Smo
973 A1 and Smo Δ570-581. (C) Bar graph of PTZ cumulative dose needed to induce generalized tonic-
974 clonic seizures. Bars are medians with experimental points. Mann-Whitney test. Numbers in
975 parenthesis indicate the number of rats used. *$p < 0.05$; **$p < 0.01$.
976
977 **Figure 6: Smo signaling controls chloride homeostasis in vitro.** (A) Gramicidin perforated patch
978 clamp recordings I-V relationships for isoguvacine currents in mCherry (left panel) or KCC2-pH_{ext}
979 (right panel) with or without Smo A1 or Smo Δ570-581 in hippocampal primary neuronal cultures (9
980 DIV). Inserts depict the isoguvacine currents for CTRL condition. Scale bar, 500 ms, 50 pA. (B) Box
981 plots of E_{GABA} in the indicated conditions. Mann-Whitney test. The number of cells recorded and
982 cultures used are indicated in parenthesis. *$p < 0.05$; ** $p < 0.01$; ***$p < 0.001$.
983
984 **Figure 7: Dominant negative form of Smo affects the stability of KCC2 to the plasmalemmal**
985 **surface.** (A) Scheme of the multistep immunolabeling protocol applied to 9 DIV neurons. First Ab,
986 primary antibody; second Cy3, Cy3-conjugated secondary antibody; second Alexa 647, Alexa Fluor
987 647–conjugated secondary antibody; PFA, paraformaldehyde. The scheme does not include final steps
988 of fixed and permeabilized cells labeled with mouse anti-GFP and anti-mouse Alexa Fluor 488
989 antibody [total protein pool (Ft)]. (B) Representative images illustrating total, membrane and
990 internalized pools of KCC2 with external tag (KCC2-pHext) in vehicle, and Smo-related transfected
991 constructs in hippocampal primary culture neurons. A KCC2 construction stable to membrane (A/A
992 KCC2) was used as positive control for KCC2 membrane trafficking. Neurons expressing a KCC2
993 mutant construction not addressed to membrane (ΔNTD-KCC2) were proceeded in parallel
994 experiments to ensure that immunocytochemistry on living neurons does not permeabilized the

995 membrane. Scale bars 20µm. (C) Box plots of total protein (F_t), (D) normalized membrane (F_m), (E)
996 internalized pool (F_i) fluorescence and (F) single membrane cluster size in cultured neurons expressing
997 the indicated constructs. Mann-Whitney test. The number of cells and cultures used indicated in
998 parenthesis are identical for all box plots. The samples size are the same for all boxplots. *p <0.05,
999 **p < 0.01, ***p<0.005, ****p<0.001.
1000
1001

Fig. 1

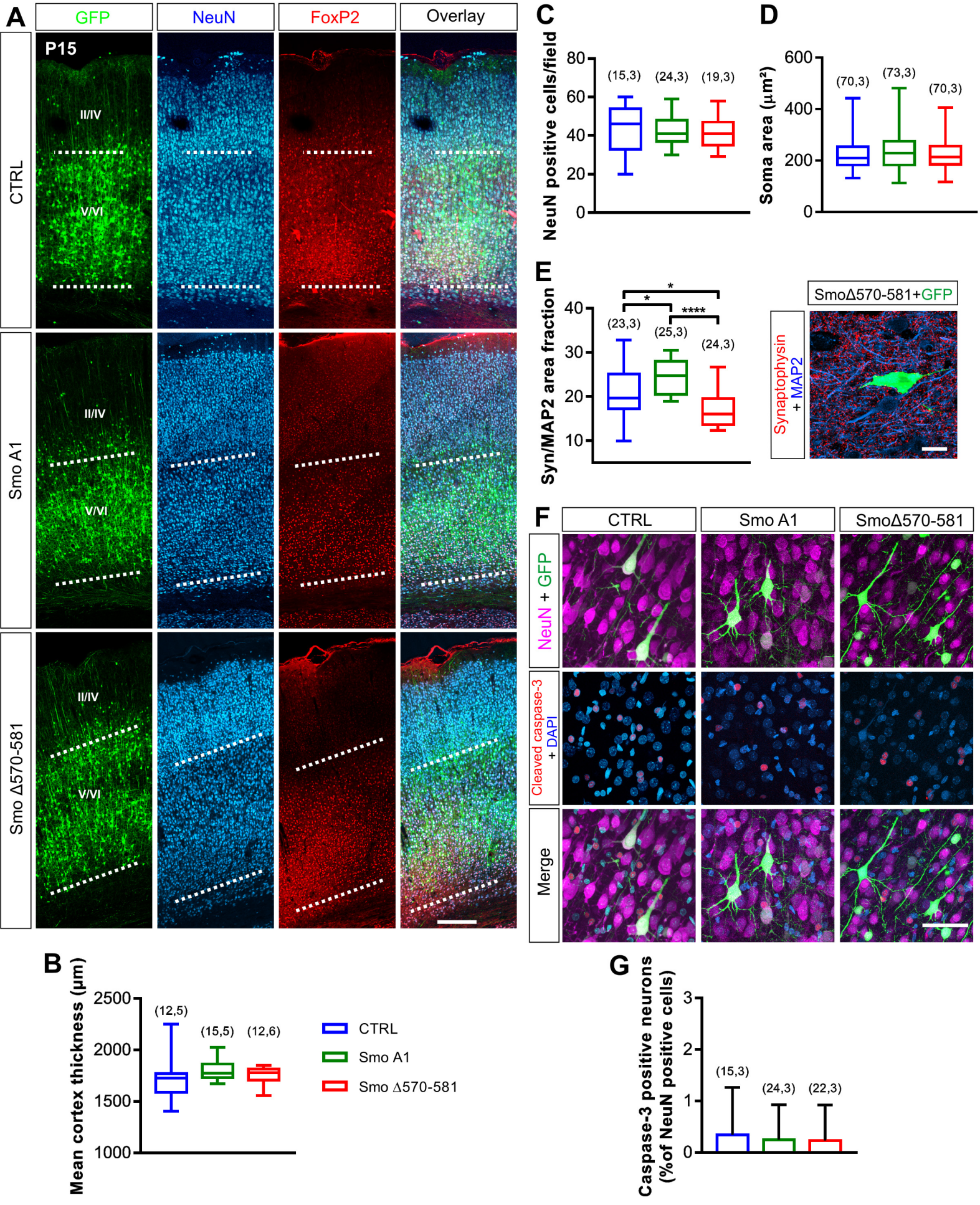
A
GFP
NeuN
FoxP2
Overlay
P15
CTRL
Smo A1
Smo Δ570-581
II/IV
V/VI
B
Mean cortex thickness (µm)
2500
2000
1500
1000
(12,5)
(15,5)
(12,6)
CTRL
Smo A1
Smo Δ570-581
C
NeuN positive cells/field
80
60
40
20
0
(15,3)
(24,3)
(19,3)
D
Soma area (µm²)
600
400
200
0
(70,3)
(73,3)
(70,3)
E
Syn/MAP2 area fraction
40
30
20
10
(23,3)
(25,3)
(24,3)
*
*
****
SmoΔ570-581+GFP
Synaptophysin + MAP2
F
CTRL
Smo A1
SmoΔ570-581
NeuN + GFP
Cleaved caspase-3 + DAPI
Merge
G
Caspase-3 positive neurons (%of NeuN positive cells)
3
2
1
0
(15,3)
(24,3)
(22,3)

Figure 2

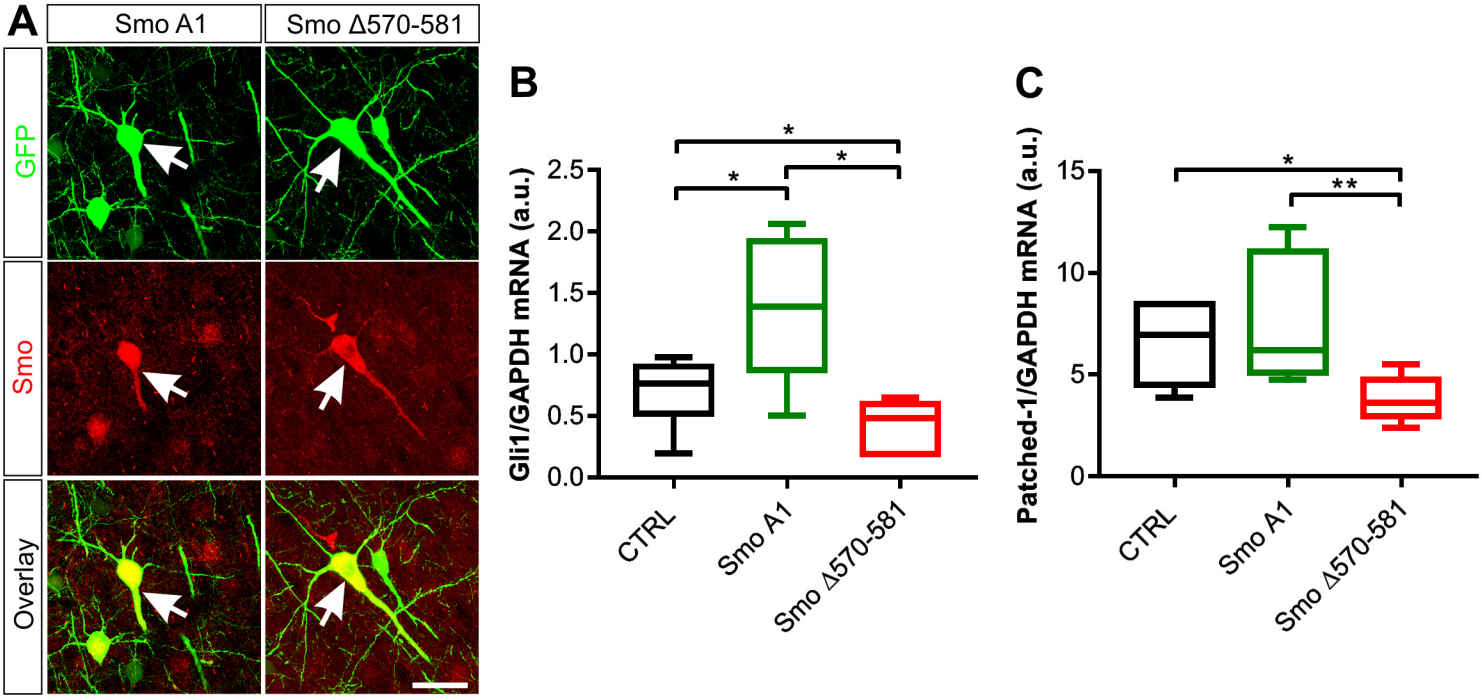
A
Smo A1
Smo Δ570-581
GFP
Smo
Overlay
B
Gli1/GAPDH mRNA (a.u.)
2.5
2.0
1.5
1.0
0.5
0.0
*
*
*
CTRL
Smo A1
Smo Δ570-581
C
Patched-1/GAPDH mRNA (a.u.)
15
10
5
0
*
**
CTRL
Smo A1
Smo Δ570-581

Figure 3

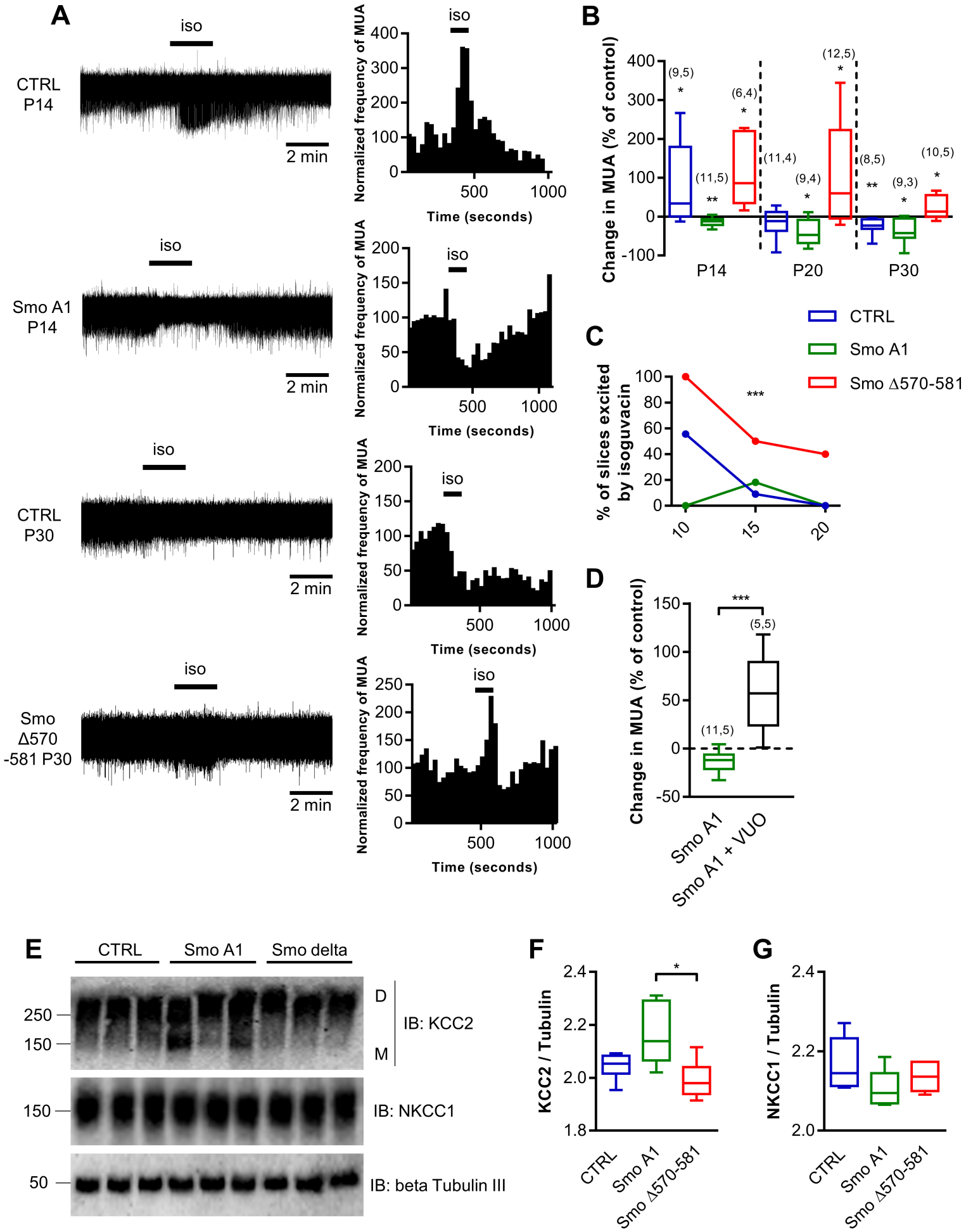
A
iso
CTRL P14
2 min
Smo A1 P14
CTRL P30
Smo Δ570 -581 P30
Normalized frequency of MUA
Time (seconds)
B
Change in MUA (% of control)
P14
P20
P30
(9,5)
(11,5)
(6,4)
(11,4)
(9,4)
(12,5)
(8,5)
(9,3)
(10,5)
C
% of slices excited by isoguvacin
CTRL
Smo A1
Smo Δ570-581
D
Smo A1
Smo A1 + VUO
(5,5)
E
CTRL
Smo A1
Smo delta
250
150
50
D
M
IB: KCC2
IB: NKCC1
IB: beta Tubulin III
F
KCC2 / Tubulin
G
NKCC1 / Tubulin

Figure 4

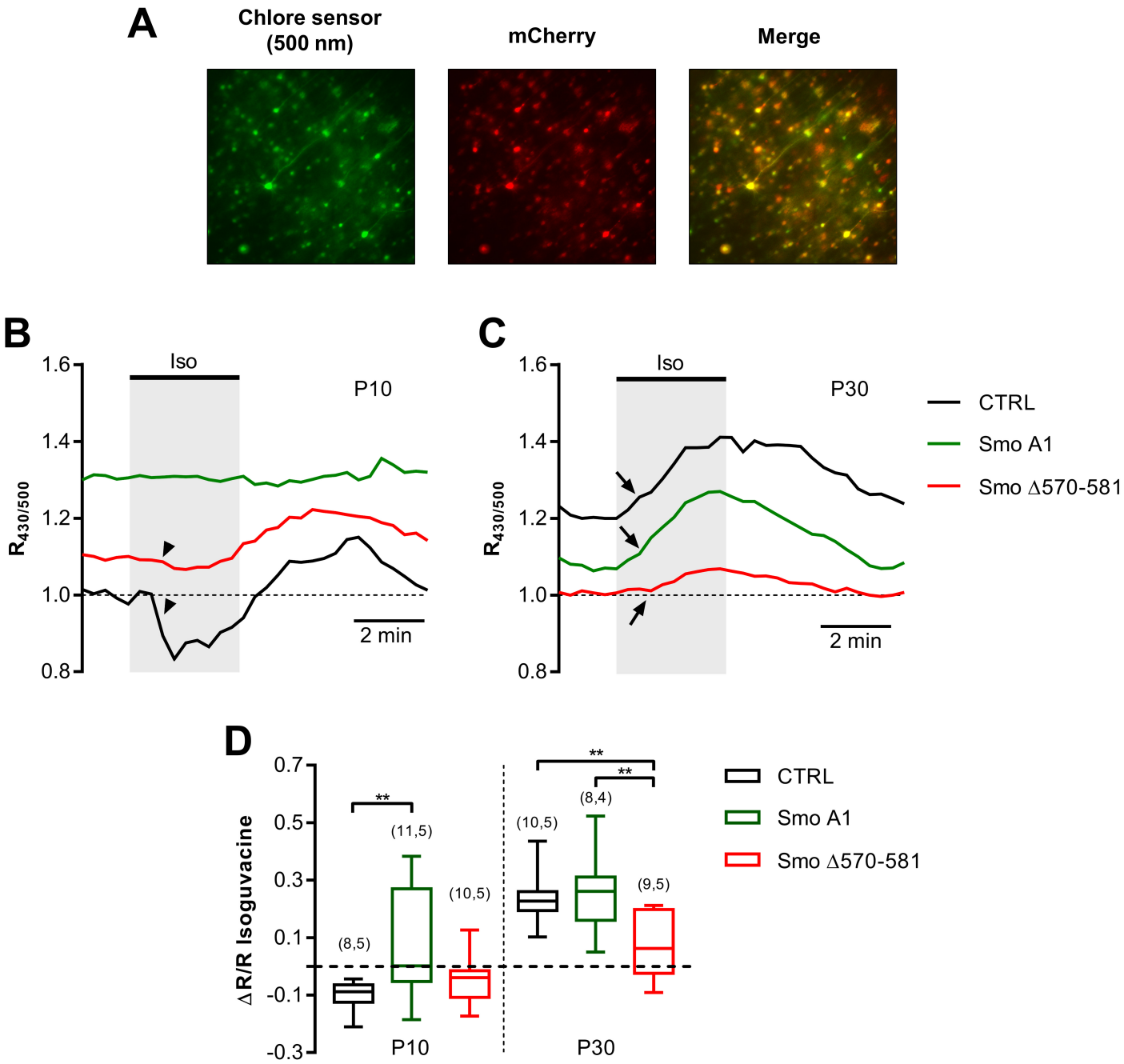
A
Chlore sensor (500 nm)
mCherry
Merge
B
Iso
P10
1.6
1.4
1.2
1.0
0.8
R430/500
2 min
C
Iso
P30
1.6
1.4
1.2
1.0
0.8
R430/500
2 min
CTRL
Smo A1
Smo Δ570-581
D
ΔR/R Isoguvacine
0.7
0.5
0.3
0.1
-0.1
-0.3
**
(8,5)
(11,5)
(10,5)
(10,5)
(8,4)
(9,5)
P10
P30
CTRL
Smo A1
Smo Δ570-581

Figure 5

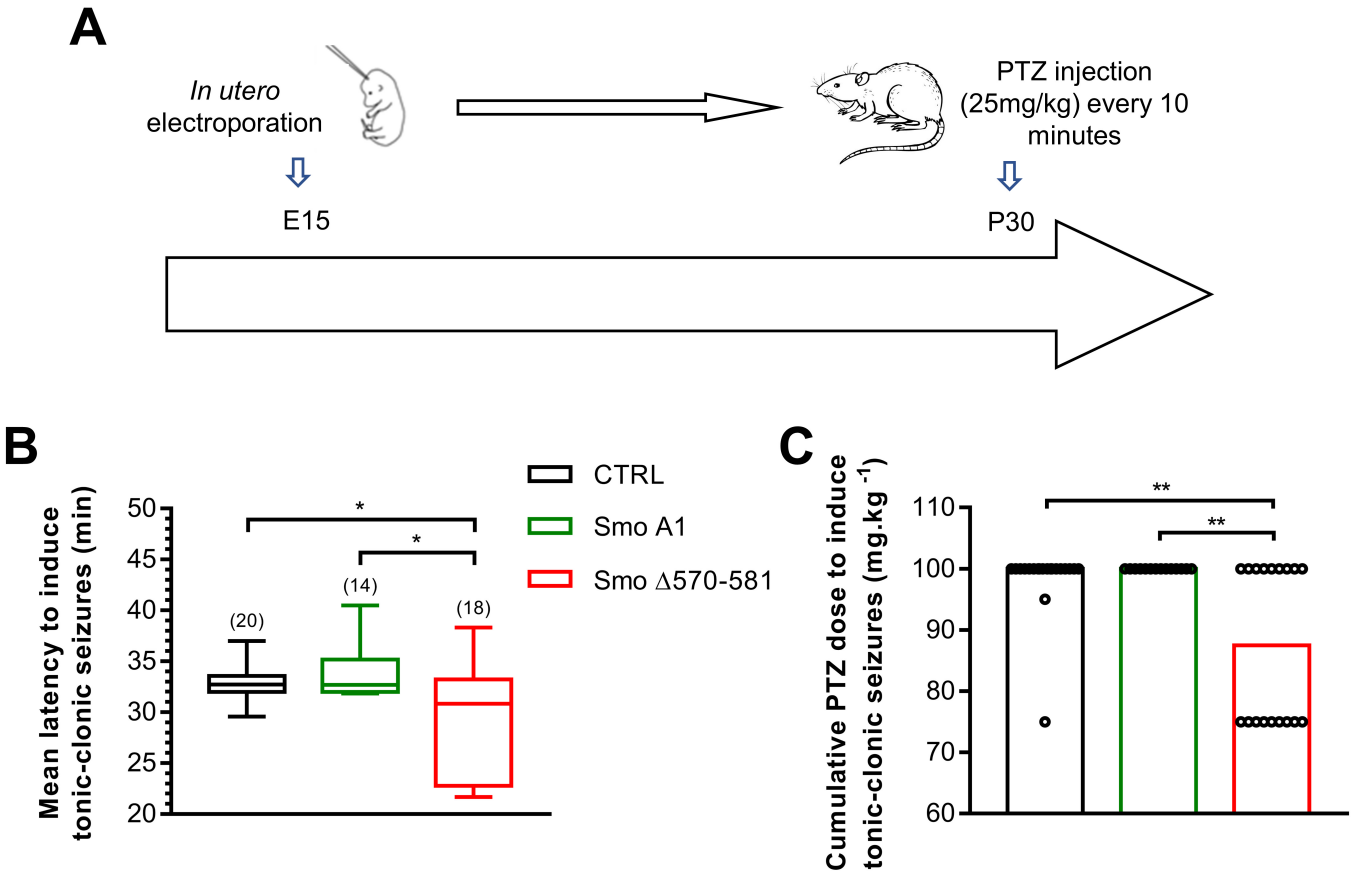
A
In utero
electroporation
E15
PTZ injection
(25mg/kg) every 10
minutes
P30
B
Mean latency to induce
tonic-clonic seizures (min)
50
45
40
35
30
25
20
*
*
(20)
(14)
(18)
CTRL
Smo A1
Smo Δ570-581
C
Cumulative PTZ dose to induce
tonic-clonic seizures (mg.kg -1)
110
100
90
80
70
60
**
**

Figure 6

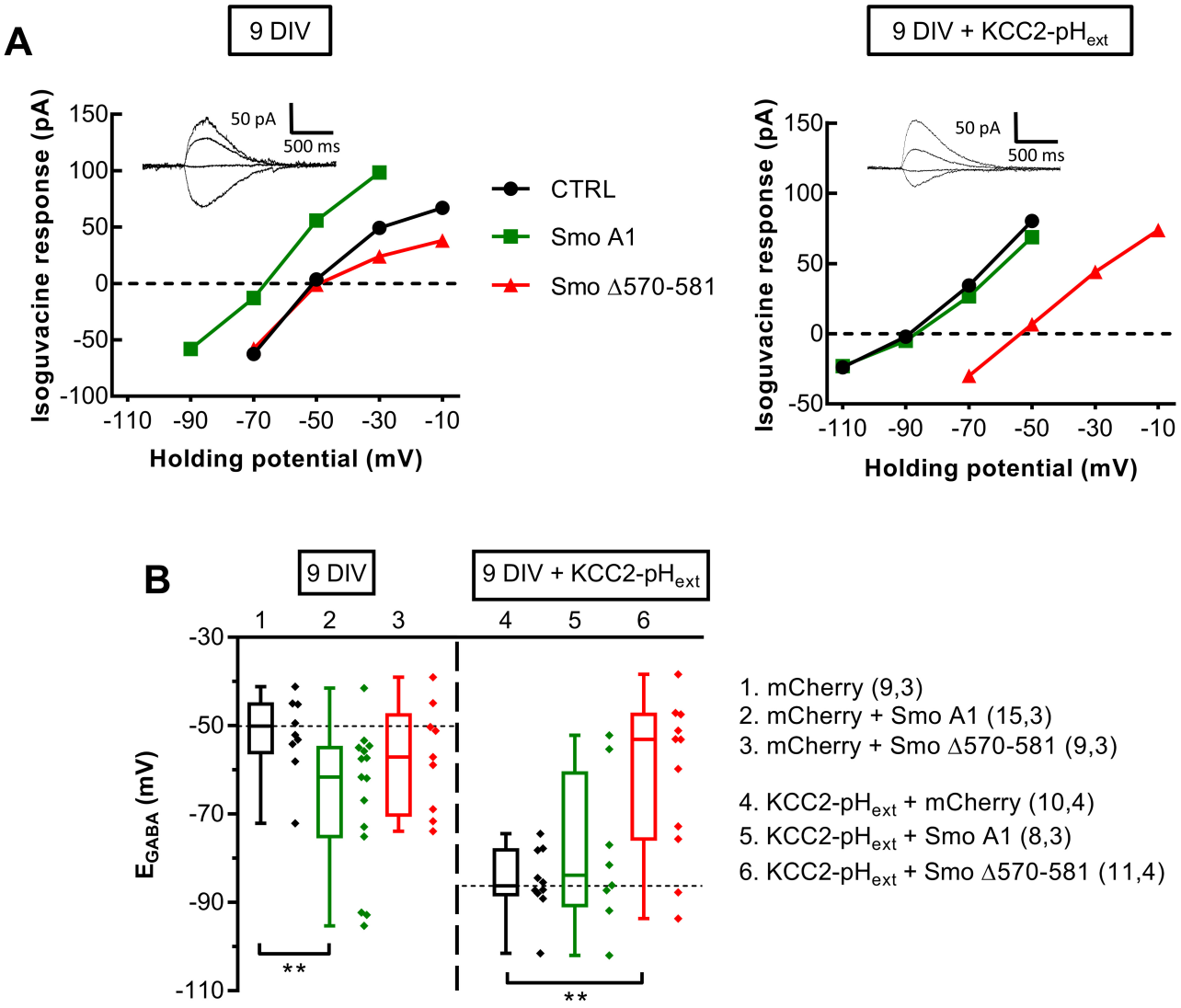
A
9 DIV
9 DIV + KCC2-pH$_{ext}$
Isoguvacine response (pA)
Holding potential (mV)
50 pA
500 ms
CTRL
Smo A1
Smo Δ570-581
B
E_{GABA} (mV)
**
1. mCherry (9,3)
2. mCherry + Smo A1 (15,3)
3. mCherry + Smo Δ570-581 (9,3)
4. KCC2-pH$_{ext}$ + mCherry (10,4)
5. KCC2-pH$_{ext}$ + Smo A1 (8,3)
6. KCC2-pH$_{ext}$ + Smo Δ570-581 (11,4)

Figure 7

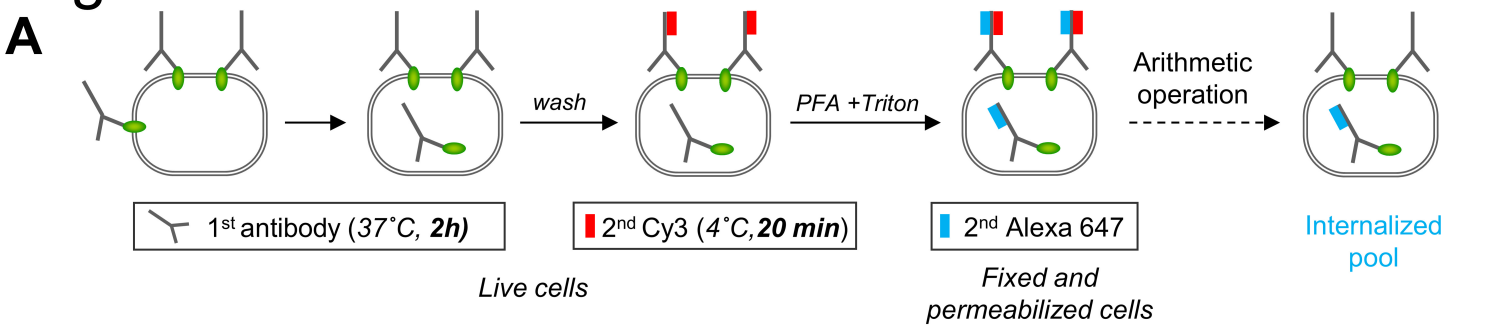
A
wash
PFA +Triton
Arithmetic operation
1st antibody (37˚C, 2h)
2nd Cy3 (4˚C, 20 min)
2nd Alexa 647
Internalized pool
Live cells
Fixed and permeabilized cells

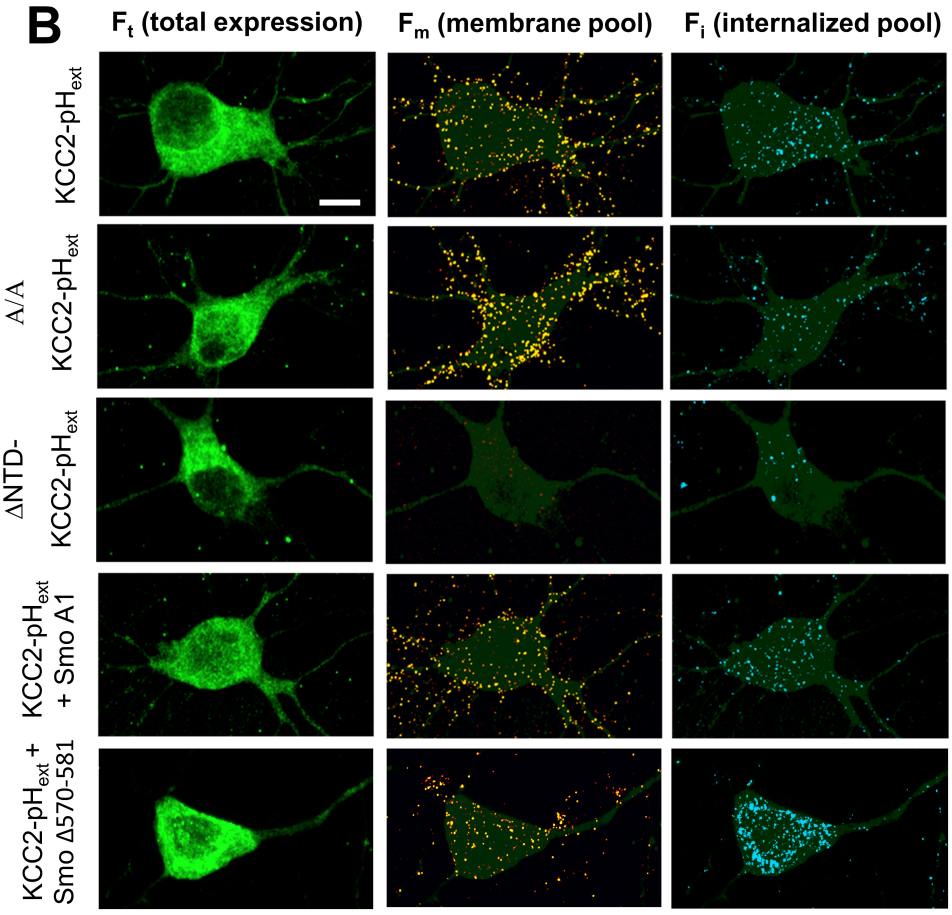
B
Ft (total expression)
Fm (membrane pool)
Fi (internalized pool)
KCC2-pHext
A/A KCC2-pHext
ΔNTD-KCC2-pHext
KCC2-pHext + Smo A1
KCC2-pHext + Smo Δ570-581

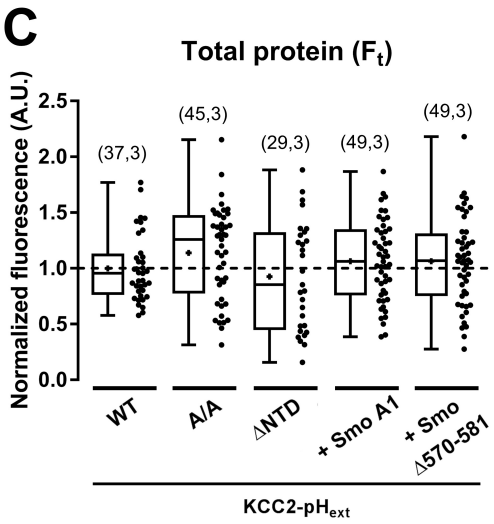
C
Total protein (Ft)
Normalized fluorescence (A.U.)
(37,3)
(45,3)
(29,3)
(49,3)
(49,3)
WT
A/A
ΔNTD
+ Smo A1
+ Smo Δ570-581
KCC2-pHext

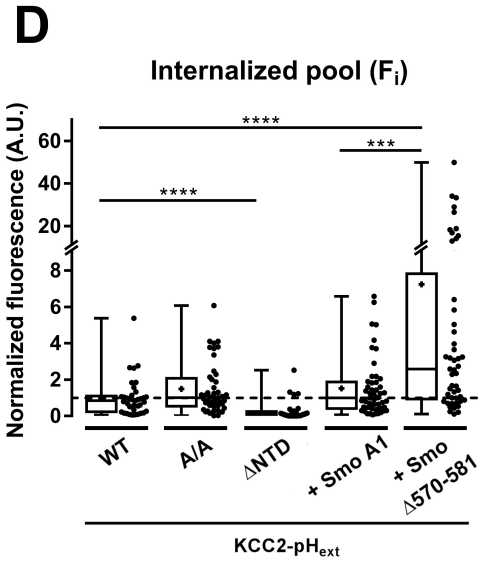
D
Internalized pool (Fi)
Normalized fluorescence (A.U.)
****
***
****
WT
A/A
ΔNTD
+ Smo A1
+ Smo Δ570-581
KCC2-pHext

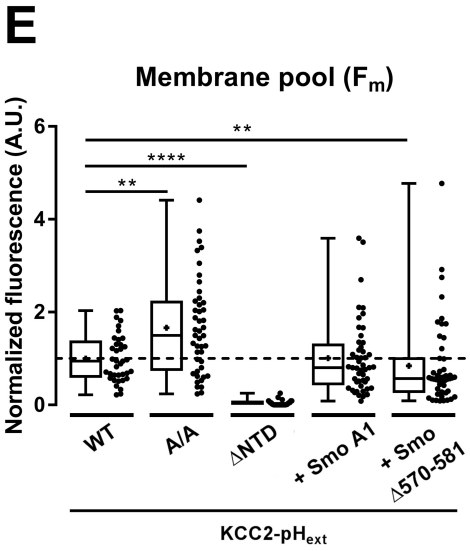
E
Membrane pool (Fm)
Normalized fluorescence (A.U.)
**
****
**
WT
A/A
ΔNTD
+ Smo A1
+ Smo Δ570-581
KCC2-pHext

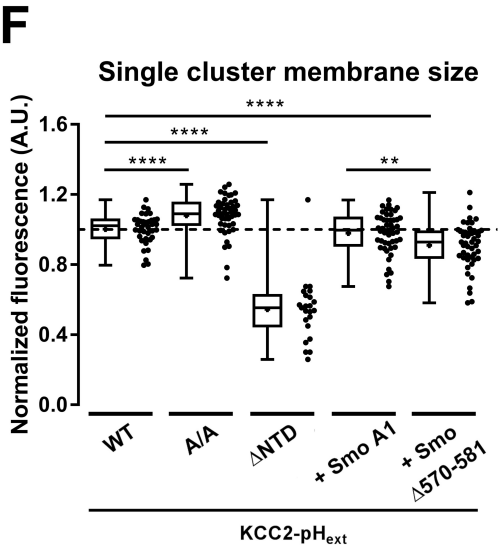
F
Single cluster membrane size
Normalized fluorescence (A.U.)
****
****
****
**
WT
A/A
ΔNTD
+ Smo A1
+ Smo Δ570-581
KCC2-pHext

Figure	Data structure	Data type	Group (n)	Type of Test	Power, statistical significance
1B	Non-normal distribution	Boxplot	CTRL (12) vs Smo A1 (15)	Mann-Whitney	U=53, p=0.074
			CTRL (12) vs Smo Δ570-581 (12)	Mann-Whitney	U=48, p=0.178
			Smo A1 (15) vs Smo Δ570-581 (12)	Mann-Whitney	U=78, p=0.580
1C	Non-normal distribution	Boxplot	CTRL (15) vs Smo A1 (24)	Mann-Whitney	U=167.5, p=0.726
			CTRL (15) vs Smo Δ570-581 (19)	Mann-Whitney	U=120, p=0.444
			Smo A1 (24) vs Smo Δ570-581 (19)	Mann-Whitney	U=199, p=0.485
1D	Non-normal distribution	Boxplot	CTRL (70) vs Smo A1 (73)	Mann-Whitney	U=2255, p=0.226
			CTRL (70) vs Smo Δ570-581 (70)	Mann-Whitney	U=2282, p=0.485
			Smo A1 (73) vs Smo Δ570-581 (70)	Mann-Whitney	U=2431, p=0.618
1E	Non-normal distribution	Boxplot	CTRL (23) vs Smo A1 (25)	Mann-Whitney	U=167, p=0.012
			CTRL (23) vs Smo Δ570-581 (24)	Mann-Whitney	U=160, p=0.013
			Smo A1 (25) vs Smo Δ570-581 (24)	Mann-Whitney	U=37, p<0.0001
1G	Non-normal distribution	mean ± SD	CTRL (15) vs Smo A1 (24)	Mann-Whitney	U=176.5, p=0.704
			CTRL (15) vs Smo Δ570-581 (19)	Mann-Whitney	U=137.5, p=0.741
			Smo A1 (24) vs Smo Δ570-581 (19)	Mann-Whitney	U=224.5, p=0.928
2B	Non-normal distribution	Boxplot	CTRL (6) vs Smo A1 (6)	Mann-Whitney	U=5, p=0.041
			CTRL (6) vs Smo Δ570-581 (6)	Mann-Whitney	U=5, p=0.039
			Smo A1 (6) vs Smo Δ570-581 (6)	Mann-Whitney	U=3, p=0.015
2C	Non-normal distribution	Boxplot	CTRL (6) vs Smo A1 (6)	Mann-Whitney	U=15, p=0.666
			CTRL (6) vs Smo Δ570-581 (6)	Mann-Whitney	U=4, p=0.026
			Smo A1 (6) vs Smo Δ570-581 (6)	Mann-Whitney	U=2, p=0.008
3B	Non-normal distribution	Boxplot	CTRL P14 (9)	Wilcoxon test	rank sum=39, p=0.019

			Smo A1 P14 (11)	Wilcoxon test	rank sum=-54, *p*=0.009
			Smo Δ570-581 P14 (6)	Wilcoxon test	rank sum=21, *p*=0.031
			CTRL P20 (11)	Wilcoxon test	rank sum=-16, *p*=0.519
			Smo A1 P20 (9)	Wilcoxon test	rank sum=-41, *p*=0.011
			Smo Δ570-581 P20 (12)	Wilcoxon test	rank sum=52, *p*=0.042
			CTRL P30 (8)	Wilcoxon test	rank sum=-36, *p*=0.007
			Smo A1 P30 (9)	Wilcoxon test	rank sum=-34, *p*=0.015
			Smo Δ570-581 P30 (10)	Wilcoxon test	rank sum=41, *p*=0.037
3C	Non-normal distribution	percentage		Chi square test	CR(4)=67.13, *p*<0.0001
3D	Non-normal distribution	Boxplot	Smo A1 (11) vs Smo A1 + VU0 (5)	Mann-Whitney	*U*= 1, *p*=0.0009
3F	Non-normal distribution	Boxplot	CTRL (6) vs Smo A1 (6)	Mann-Whitney	*U*=6, *p*=0.064
			CTRL (6) vs Smo Δ570-581 (6)	Mann-Whitney	*U*=8, *p*=0.132
			Smo A1 (6) vs Smo Δ570-581 (6)	Mann-Whitney	*U*=2, *p*=0.008
3G	Non-normal distribution	Boxplot	CTRL (6) vs Smo A1 (6)	Mann-Whitney	*U*=7, *p*=0.093
			CTRL (6) vs Smo Δ570-581 (6)	Mann-Whitney	*U*=13, *p*=0.484
			Smo A1 (6) vs Smo Δ570-581 (6)	Mann-Whitney	U=10, p=0.240
4D	Non-normal distribution	Boxplot	CTRL P14 (8) vs Smo A1 P14 (11)	Mann-Whitney	U=11, p=0.005
			CTRL P14 (8) vs Smo Δ570-581 P14 (10)	Mann-Whitney	U=24, p=0.172
			Smo A1 P14 (11) vs Smo Δ570-581 P14 (10)	Mann-Whitney	U=32, p=0.114
			CTRL P30 (10) vs Smo A1 P30 (8)	Mann-Whitney	U=34, p=0.633
			CTRL P30 (10) vs Smo Δ570-581 P30 (9)	Mann-Whitney	U=9, p=0.002
			Smo A1 P30 (8) vs Smo Δ570-581 P30 (9)	Mann-Whitney	U=11, p=0.015

5B	Non-normal distribution	Boxplot	CTRL (20) vs Smo A1 (14)	Mann-Whitney	U=121, p=0.515
			CTRL (20) vs Smo Δ570-581 (18)	Mann-Whitney	U=110.5, p=0.041
			Smo A1 (14) vs Smo Δ570-581 (18)	Mann-Whitney	U=67, p=0.024
5C	Non-normal distribution	Boxplot	CTRL (20) vs Smo A1 (14)	Mann-Whitney	U=126, p=0.500
			CTRL (20) vs Smo Δ570-581 (18)	Mann-Whitney	U=103.5, p=0.005
			Smo A1 (14) vs Smo Δ570-581 (18)	Mann-Whitney	U=63, p=0.003
6B	Non-normal distribution	Boxplot	mCherry (9) vs KCC2+mCherry	Mann-Whitney	U=0, p<0.0001
			mCherry (9) vs mCherry+Smo A1 (15)	Mann-Whitney	U=24, p=0.008
			mCherry (9) vs mCherry+Smo Δ570-581 (9)	Mann-Whitney	U=30, p=0.386
			mCherry+Smo A1 (15) vs mCherry+Smo Δ570-581 (9)	Mann-Whitney	U=46, p=0.215
			KCC2 (10) vs KCC2+Smo A1 (8)	Mann-Whitney	U=35, p=0.696
			KCC2 (10) vs KCC2+Smo Δ570-581 (8)	Mann-Whitney	U=17, p=0.006
			KCC2+Smo A1 (8) vs KCC2+Smo Δ570-581 (8)	Mann-Whitney	U=21, p=0.062
7C	Non-normal distribution	Boxplot	WT (37) vs A/A (45)	Mann-Whitney	U=648, p=0.086
			WT (37) vs ΔNTD (29)	Mann-Whitney	U=469, p=0.389
			WT (37) vs +Smo A1 (49)	Mann-Whitney	U=784, p=0.288
			WT (37) vs +Smo Δ570-581 (49)	Mann-Whitney	U=790, p=0.313
			+ Smo A1 (49) vs +Smo Δ570-581 (49)	Mann-Whitney	U=1198, p=0.988
7D	Non-normal distribution	Boxplot	WT (37) vs A/A (45)	Mann-Whitney	U=647, p=0.084
			WT (37) vs ΔNTD (29)	Mann-Whitney	U=201, p<0.0001
			WT (37) vs +Smo A1 (49)	Mann-Whitney	U=741, p=0.150

			WT (37) vs +Smo Δ570-581 (49)	Mann-Whitney	U=390, p<0.0001
			+ Smo A1 (49) vs +Smo Δ570-581 (49)	Mann-Whitney	U=682, p=0.0002
7E	Non-normal distribution	Boxplot	WT (37) vs A/A (45)	Mann-Whitney	U=508, p=0.002
			WT (37) vs ΔNTD (29)	Mann-Whitney	U=2, p<0.0001
			WT (37) vs +Smo A1 (49)	Mann-Whitney	U=810, p=0.404
			WT (37) vs +Smo Δ570-581 (49)	Mann-Whitney	U=608, p=0.008
			+ Smo A1 (49) vs +Smo Δ570-581 (49)	Mann-Whitney	U=944, p=0.068
7F	Non-normal distribution	Boxplot	WT (37) vs A/A (45)	Mann-Whitney	U=420, p<0.0001
			WT (37) vs ΔNTD (29)	Mann-Whitney	U=37, p<0.0001
			WT (37) vs +Smo A1 (49)	Mann-Whitney	U=647, p=0.478
			WT (37) vs +Smo Δ570-581 (49)	Mann-Whitney	U=480, p<0.0001
			+ Smo A1 (49) vs +Smo Δ570-581 (49)	Mann-Whitney	U=785, p=0.002